iScience

CellPress
OPEN ACCESS

Article

The Oscillation Amplitude, Not the Frequency of Cytosolic Calcium, Regulates Apoptosis Induction

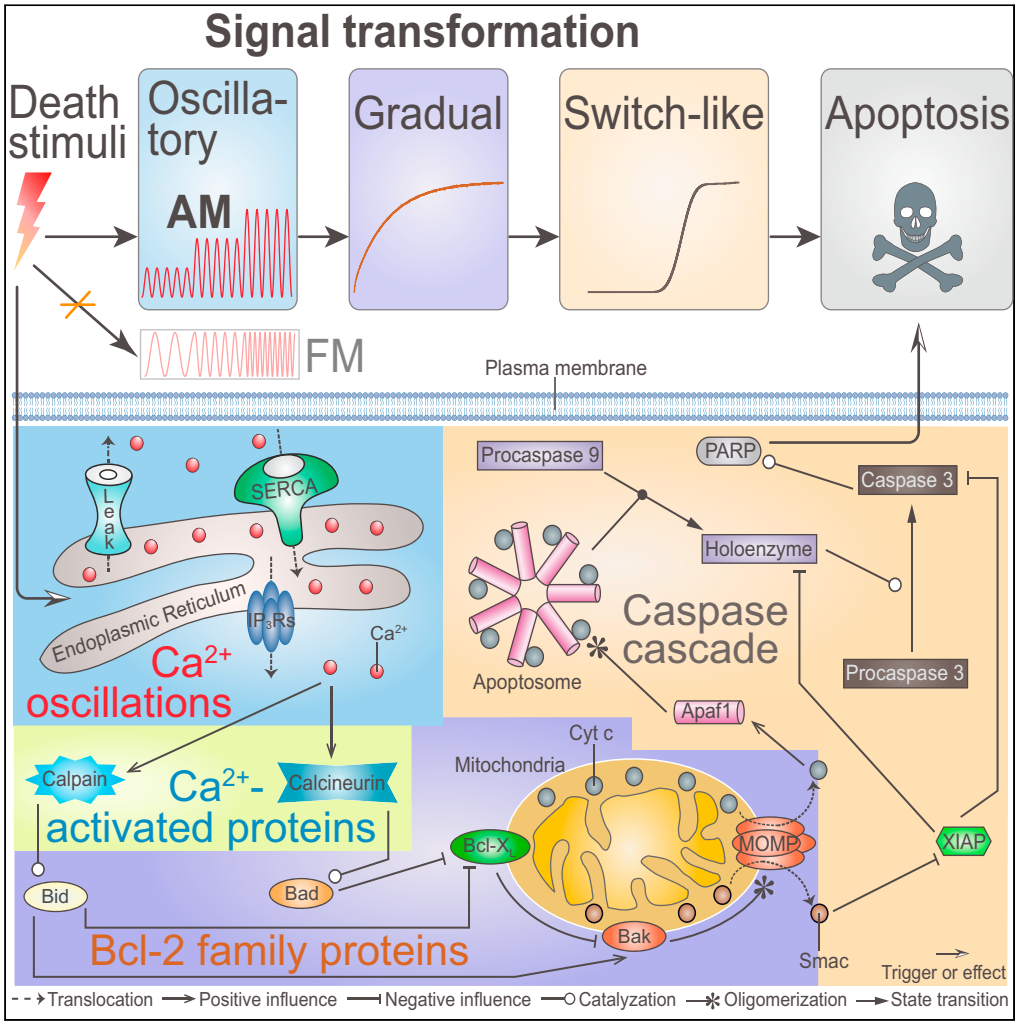

Hong Qi, Xiang Li, Zhen Jin, Thomas Simmen, Jianwei Shuai

hongqi@sxu.edu.cn (H.Q.)
jianweishuai@xmu.edu.cn (J.S.)

HIGHLIGHTS

A signaling network of cytosolic Ca^{2+}-induced apoptosis is constructed

The network is converted into a mathematical model composed of four modules

Oscillatory signals first transform into gradual ones and then into switch-like ones

Ca^{2+} regulates apoptosis mainly via amplitude, rather than frequency, modulation

Qi et al., iScience 23, 101671
November 20, 2020
https://doi.org/10.1016/j.isci.2020.101671

iScience

CellPress
OPEN ACCESS

Article

The Oscillation Amplitude, Not the Frequency of Cytosolic Calcium, Regulates Apoptosis Induction

Hong Qi,[1,2,*] Xiang Li,[3,4,5] Zhen Jin,[1,2] Thomas Simmen,[6] and Jianwei Shuai[3,4,5,7,*]

SUMMARY

Although a rising concentration of cytosolic Ca^{2+} has long been recognized as an essential signal for apoptosis, the dynamical mechanisms by which Ca^{2+} regulates apoptosis are not clear yet. To address this, we constructed a computational model that integrates known biochemical reactions and can reproduce the dynamical behaviors of Ca^{2+}-induced apoptosis as observed in experiments. Model analysis shows that oscillating Ca^{2+} signals first convert into gradual signals and eventually transform into a switch-like apoptotic response. Via the two processes, the apoptotic signaling pathway filters the frequency of Ca^{2+} oscillations effectively but instead responds acutely to their amplitude. Collectively, our results suggest that Ca^{2+} regulates apoptosis mainly via oscillation amplitude, rather than frequency, modulation. This study not only provides a comprehensive understanding of how oscillatory Ca^{2+} dynamically regulates the complex apoptotic signaling network but also presents a typical example of how Ca^{2+} controls cellular responses through amplitude modulation.

INTRODUCTION

Calcium ion (Ca^{2+}) is one of the most versatile and universal signaling agents to translate extra- and intracellular information into specific cellular outcomes (Berridge et al., 1998; Giorgi et al., 2018a). Upon stimulation, Ca^{2+} is released from the endoplasmic reticulum (ER) into the cytosol through inositol 1,4,5-trisphosphate receptor (IP_3R) channels. Changes in cytosolic Ca^{2+} concentration ($[Ca^{2+}]$) of a moderate level can govern a myriad of vital cell functions, including fertilization, proliferation, and differentiation, and are essential for cell survival (Berridge et al., 2003). However, excessive elevations of $[Ca^{2+}]$ typically result in cell death, including apoptosis (Orrenius et al., 2003).

A cytosolic Ca^{2+} overload initiates the mitochondrial apoptotic pathway as follows. Ca^{2+} can activate calpain and calcineurin, causing the activation of BH3-only proteins (Chen et al., 2001; Wang et al., 1999). This results in the sequestering of anti-apoptotic Bcl-2 proteins and the activation of the pro-apoptotic effectors Bax and Bak (Czabotar et al., 2014; Youle and Strasser, 2008). These interaction patterns among Bcl-2 protein family culminate in Bax and Bak oligomerization and mitochondrial outer membrane permeabilization (MOMP) (Tait and Green, 2010). Subsequently, several apoptogenic factors are released from the mitochondrial intermembrane space, particularly cytochrome c (Cyt c) (Ow et al., 2008). In the cytosol, Cyt c engages Apaf1 and forms the apoptosome, which recruits caspase 9 and promotes caspase 3 activation. Active caspase 3 cleaves several hundred proteins, resulting in apoptosis (Shi, 2004). In addition, mitochondria retain cytosolic Ca^{2+} and this massive mitochondrial Ca^{2+} accumulation causes the opening of mitochondrial permeability transition pore, which leads to the Cyt c release and cell death (Qi and Shuai, 2016). Despite this detailed characterization of the molecular sequence of events, we still lack a comprehensive understanding of how Ca^{2+} dynamics control this complex apoptosis signaling network.

Differential equation modeling can simulate the dynamic output of individual proteins and can identify critical players in a signaling network, thus often providing novel insights to our understanding of cellular dynamics (Spencer and Sorger, 2011; Yao et al., 2016). Such modeling efforts have been devoted to understand intracellular Ca^{2+} dynamics (Dupont and Sneyd, 2017; Goldbeter et al., 1990; Li and Rinzel, 1994; Qi et al., 2015; Shuai and Jung, 2003; Sneyd et al., 2017) and the mechanistic details of the apoptotic pathway (Albeck et al., 2008; Anderson et al., 2019; Legewie et al., 2006; Qi et al., 2018; Rehm et al.,

[1]Complex Systems Research Center, Shanxi University, Taiyuan 030006, China

[2]Shanxi Key Laboratory of Mathematical Techniques and Big Data Analysis on Disease Control and Prevention, Shanxi University, Taiyuan 030006, China

[3]Department of Physics, Xiamen University, Xiamen 361005, China

[4]State Key Laboratory of Cellular Stress Biology, Innovation Center for Cell Signaling Network, Xiamen University, Xiamen 361102, China

[5]National Institute for Data Science in Health and Medicine, Xiamen University, Xiamen 361102, China

[6]Faculty of Medicine and Dentistry, Department of Cell Biology, University of Alberta, Edmonton, AB T6G2H7, Canada

[7]Lead Contact

*Correspondence: hongqi@sxu.edu.cn (H.Q.), jianweishuai@xmu.edu.cn (J.S.)

https://doi.org/10.1016/j.isci.2020.101671

2006; Santos et al., 2019; Spencer and Sorger, 2011; Yin et al., 2017; Zhao et al., 2015). However, so far, Ca^{2+} signaling has not been mathematically integrated into models of apoptosis yet.

Two major types of Ca^{2+} temporal profiles have been reported in apoptotic cells, including a high plateau and oscillations (Boehning et al., 2003; Lee et al., 2010; Garcia et al., 2017). Oscillations of [Ca^{2+}] in individual cells often occur as repetitive spikes or sinusoid-like oscillations (Berridge, 1990; Oancea and Meyer, 1998). In our study, we focused on investigating how cytosolic Ca^{2+} oscillations, especially sinusoidal oscillations, regulate apoptosis from a network dynamics perspective.

Typically, Ca^{2+} oscillations occur with periods from seconds to minutes (Uhlén and Fritz, 2010), whereas the apoptotic program normally takes between a few and several tens of hours (Garcia et al., 2017; Márquez-Jurado et al., 2018). Owing to technical limitations in producing distinct long-term Ca^{2+} oscillations in experimental setups of apoptotic processes, the switch from a fast oscillatory Ca^{2+} signal to a switch-like apoptotic response with a long latency remains unclear.

Ca^{2+} oscillations contain information in their amplitude and frequency, thus providing two ways to selectively activate downstream signaling pathways (Berridge, 1997; Parekh, 2011). It has been shown that some gene expression events (Li et al., 1998) and the activations of CaMKII (De Koninck and Schulman, 1998), PKC (Oancea and Meyer, 1998), and Ras (Kupzig et al., 2005), as well as ATP production (Hajnóczky et al., 1995), are regulated by the frequency of Ca^{2+} oscillations. These experimental observations, together with a well-known engineering principle that frequency modulation (FM) signaling is more precise than amplitude modulation (AM) signaling, have led to the prevailing view that Ca^{2+} controls cellular functions typically by an FM mode (Dupont and Combettes, 2016; Dupont and Sneyd, 2017; Goldbeter et al., 1990; Smedler and Uhlén, 2014). We have decided to investigate whether this is also the case during Ca^{2+}-induced apoptosis.

To solve these two basic issues, we constructed a four-module network model, including Ca^{2+} oscillations, Ca^{2+}-activated proteins, Bcl-2 family proteins, and Cyt c-induced caspase cascade. We transformed the biochemical reactions of the network into a set of ordinary differential equations (ODEs). The simulation results reveal that oscillatory Ca^{2+} signals will be first converted into gradual signals, i.e., the slowly and monotonically changed signals, and then be transformed into a switch-like apoptotic response. Furthermore, our results show that, with such converting processes, Ca^{2+} regulates apoptosis mainly through an AM mode, rather than through an FM mode. Our work provides crucial insight in the understanding of the modulatory role of Ca^{2+} signals on the apoptotic process.

RESULTS

Model Construction

A complete picture of the role of Ca^{2+} as a mechanistic trigger of apoptosis is still missing. Based on previous works (Albeck et al., 2008; Rehm et al., 2006) and our recent studies (Qi et al., 2018; Qi and Shuai, 2016; Yin et al., 2017), we developed an integrative signaling network comprising four modules (Figure 1): (1) ER-involved Ca^{2+} oscillations, (2) Ca^{2+}-activated proteins, (3) MOMP controlled by Bcl-2 family proteins on mitochondria, and (4) Cyt c-induced caspase cascade. The brief descriptions of each module are presented below (see details in Supplemental Information).

Extracellular stimuli result in the formation of IP_3 (inositol 1,4,5-trisphosphate), which binds to the IP_3 receptors (IP_3Rs) to release Ca^{2+} from the ER. Cytosolic Ca^{2+} oscillations derive from three mechanisms of ions exchange between the ER and the cytoplasm: IP_3Rs-mediated Ca^{2+} release from the ER into the cytosol, SERCA (sarco/ER Ca^{2+}-ATPase)-dependent Ca^{2+} uptake from the cytosol into the ER, and Ca^{2+} leakage from the ER into the cytosol (Shuai and Jung, 2003). An important machinery linking cytosolic Ca^{2+} signal and apoptosis is the activation of two Ca^{2+}-regulated enzymes, i.e., calpain and calcineurin. In the presence of high [Ca^{2+}], calcineurin dephosphorylates Bad, thus allowing Bad to inhibit the anti-apoptotic Bcl-X_L (Wang et al., 1999). Calpain, which is normally inhibited by calpastatin (Hanna et al., 2008), cleaves Bid to form truncated Bid (tBid), which in turn can directly activate Bak or inhibit Bcl-X_L that then indirectly activates Bak (Chen et al., 2001). Active Bak monomers form oligomers to trigger MOMP. Following MOMP, Smac and Cyt c are released from the mitochondria into the cytosol. In the cytosol, Cyt c binds Apaf1 to form the heptameric apoptosome, which interacts with procaspase 9 to induce the formation of holoenzyme, thereby triggering caspase 3 activation (Li et al., 2017). Caspase 3 can cleave a series of substrates

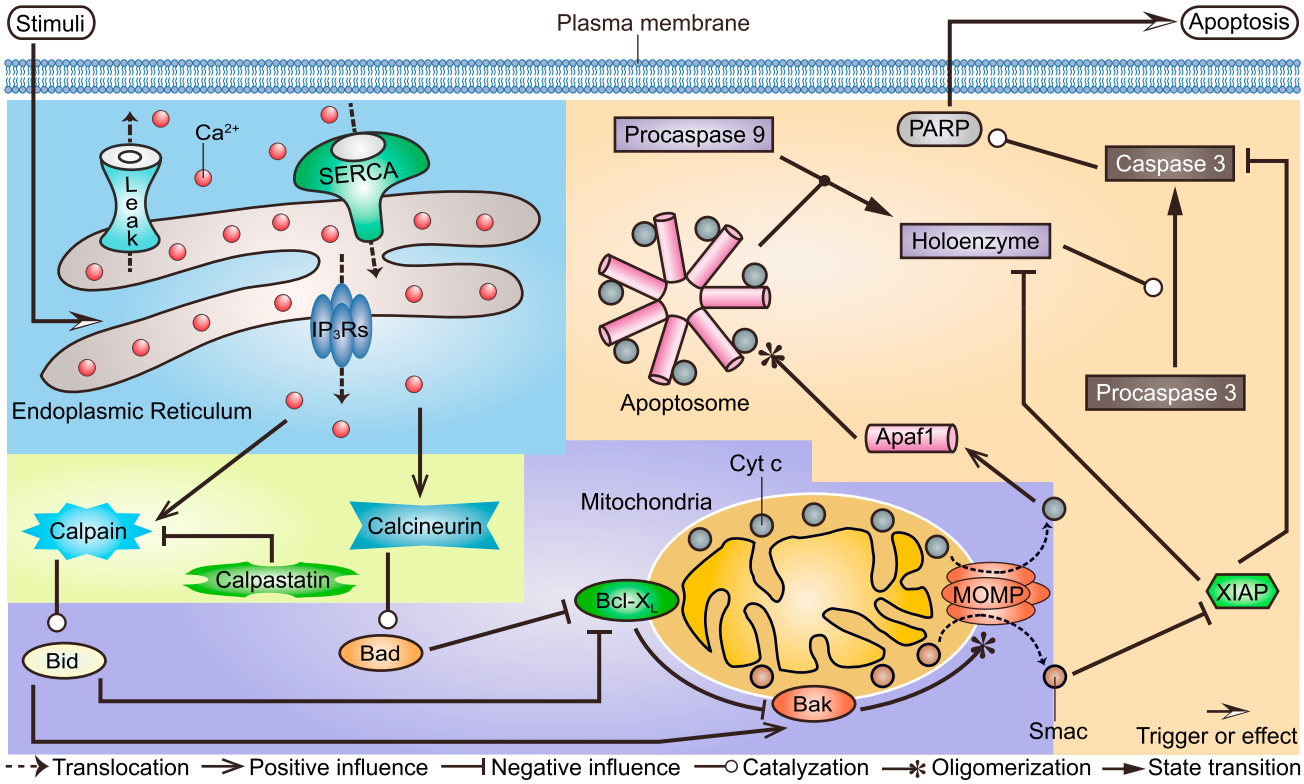

Figure 1. Model Topology Scheme

The four modules are highlighted by different background colors. The blue region is for the module of Ca^{2+} oscillations, the green for the module of Ca^{2+}-activated proteins, the purple for the module of MOMP controlled by Bcl-2 family proteins, and the yellow for the module of the Cyt c-induced caspase cascade. More details can be found in the main text.

(a process represented in the model by cleavage of PARP to form cPARP [Albeck et al., 2008]) and orchestrate the demolition of the cell. Smac assists this function by neutralizing the caspase inhibitor XIAP.

Using well-established kinetics approaches (Anderson et al., 2019; Qiao et al., 2019; Zhang et al., 2011), we translated these biochemical processes into a set of ODEs. Every variable represents the amount or concentration of a molecular species, which is dynamically controlled by the combination of all processes that increase and decrease the level of that particular molecular species. Each process is described by chemical kinetics, i.e., the mass action law or Hill function. The ODEs are numerically solved and the total simulation time was set to 18 h, the typical length of cell cycle (Spiller et al., 2010), reflecting the fact that a cell ultimately adopts one of two fates, either to survive by cell division or to die by apoptosis at the end of 18 h. In our model we assumed that the cell fate depends on the concentration of cleaved PARP ([cPARP]) within 18 h. A detailed description of all biochemical reactions, ODEs, and parameters is provided in Transparent Methods.

Dynamics of Ca^{2+} and cPARP

The simulation results we obtained are qualitatively consistent with the reported dynamics of Ca^{2+} (Dupont and Goldbeter, 1993; Gerasimenko et al., 2002; Jacob et al., 1988; Scorrano et al., 2003) and cPARP (Albeck et al., 2008; Rehm et al., 2006; Spencer and Sorger, 2011) upon incubation with apoptotic triggers. In many cell types, Ca^{2+} oscillations occur within an appropriate range of stimulus levels (Dupont and Goldbeter, 1993; Jacob et al., 1988). The time course plot (Figure 2A) and bifurcation diagram, i.e., the maximal and minimal value of Ca^{2+} oscillations (Figure 2B) show that, as the stimulus strength increases, the cytosolic Ca^{2+} changes from a stationary to an oscillatory behavior, before returning to a stationary state. The oscillation period is about 200 s (Figure 2C), as seen both in healthy and apoptotic cells (Gerasimenko et al., 2002; Scorrano et al., 2003). To define the apoptotic cell from the healthy cell, we proposed that apoptosis occurs when [cPARP] is above the apoptosis threshold of 1.02 μM, a value that corresponds to 60% substrate cleavage (dotted line in Figure 2D). This result agrees with the experimental result that apoptosis

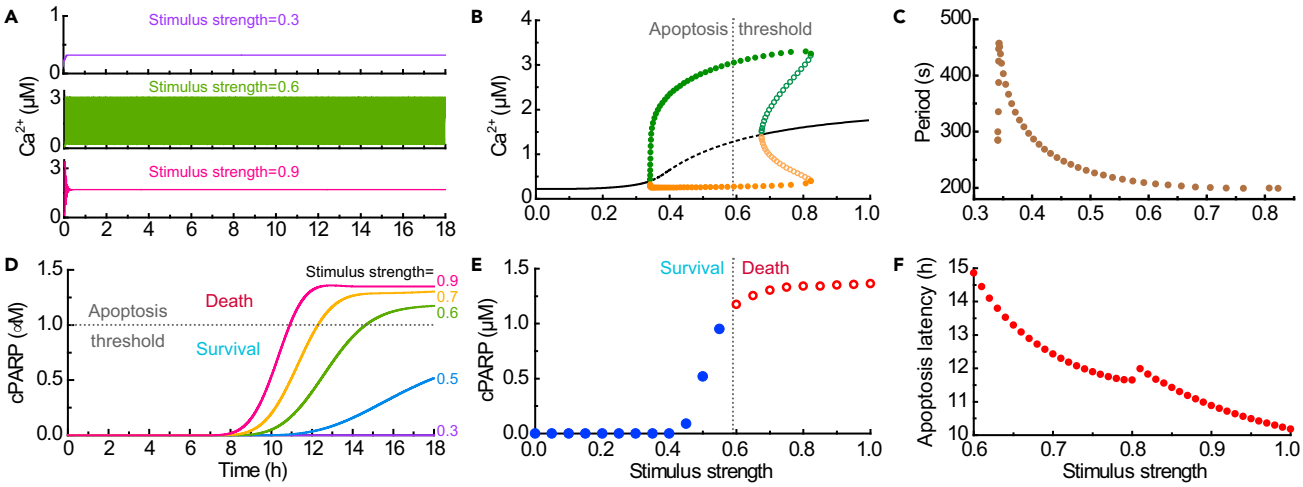

Figure 2. The Dynamical Behavior of Ca^{2+} and cPARP at Different Stimulus Strengths

(A) Different kinetic behaviors of Ca^{2+} in response to different stimuli lasting for 18 h.

(B) Bifurcation diagram of Ca^{2+} in response to different stimuli. Solid/dashed lines represent stable/unstable fixed point; filled/empty circles represent minimal (orange) and maximal (green) [Ca^{2+}] during a stable/unstable oscillation.

(C) Periods of Ca^{2+} oscillations within the stable oscillation range.

(D) The kinetic behavior of cPARP responding to different stimuli.

(E and F) The final [cPARP] (E) and the apoptosis latency (F) at different stimulus strengths.

The dotted lines in (B), (D), and (E) depict the apoptosis threshold.

is triggered only when the level of substrate cleavage exceeds a high value (Rehm et al., 2006). Accordingly, when the multiple maximal concentration of sustained Ca^{2+} oscillations exceeds a critical threshold of about 3 μM (Figure 2B), apoptosis is initiated, which is compatible with the experimental observation for [Ca^{2+}] under resting conditions and after stimulation (Giorgi et al., 2018b). Figure 2D also shows that the latency from the exposure to the apoptotic stimulus to the actual initiation of apoptosis is about 10 h, but the cleavage of PARP is sudden and switch-like, again in agreement with experimental observation (Albeck et al., 2008; Spencer and Sorger, 2011). The reasons for the selection of critical threshold of [Ca^{2+}] and [cPARP] are detailed in Supplemental Information.

It should be pointed out that, in order to provide a global view of the dynamical behavior of the system, the bifurcation diagram of Ca^{2+} is obtained mathematically with the steady states of the system (Figure 2B). However, considering the biological fact that a cell ultimately commits to apoptosis or to division at a limited time duration, we simply limited the discussion of the cell fate within 18 h for all the simulation results.

Two Indexes for Apoptosis

The relationship between the stimulus strength and the corresponding final [cPARP] yields an ultrasensitive signal-response curve (Figure 2E). Here [cPARP] at 18 h is defined as the final [cPARP], which is used as an index for cell fate. In detail, the fate of a cell is survival if the final [cPARP]<1.02 μM; otherwise, the apoptosis process is initiated. This result is insensitive to the variations in the cell cycle, i.e., total simulation time (Figure S2C). If apoptosis is triggered, another index, i.e., the apoptosis latency is introduced to evaluate how quickly apoptosis can be induced. In other words, it measures the interval between the time when the stimulus is applied and the time when the increasing [cPARP] crosses the apoptosis threshold of 1.02 μM. As shown in Figure 2F, the stronger the stimulus intensity is, the shorter the apoptosis latency becomes.

Signal Transduction

Given the different dynamics of Ca^{2+} and cPARP (Figures 2A and 2D), it is curious how the fast oscillatory Ca^{2+} signal is converted into a slow but switch-like apoptotic signal. To address this question, we analyzed the time series of the main reaction species along the reaction pathway (Figure 3A). These species include Ca^{2+}, aCalp (activated calpain), Bid, tBid, MOMP, Cyt c, holoenzyme, caspase 3, and cPARP. According to the kinetic patterns of these species, we observed that the oscillatory patterns starting with Ca^{2+} signal first become gradual for proteins such as Bid, and then become switch-like for proteins such as caspase 3.

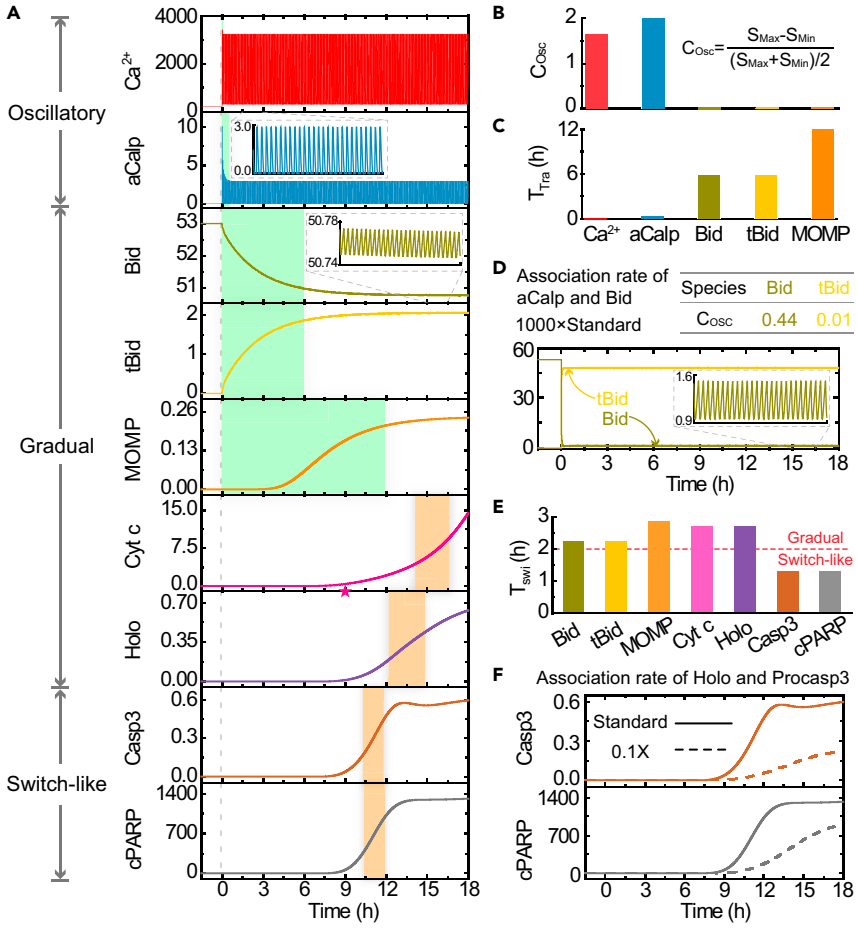

Figure 3. Transition from Oscillatory to Switch-like Kinetics

(A) Time courses of the main species in the signaling network. The vertical dashed line indicates the time at which the stimulus (strength = 0.73) is introduced. The green and orange shaded regions denote the transient time and the switch time, respectively. The time at which mitochondrial Cyt c begins to release into the cytosol is marked by an asterisk.

(B and C) (B) Oscillation coefficient (C_{Osc}) and (C) transient time (T_{Tra}) of five upstream species. S_{Max} and S_{Min} are the maximal and minimal concentrations of a certain species at the steady state, respectively.

(D) Time series and C_{Osc} of Bid and tBid with the association rate of aCalp and Bid increased by 1,000-fold.

(E) Switch time (T_{Swi}) of gradual and switch-like signals. The horizontal dashed line at 2 h is applied to distinguish the switch-like signals from the gradual ones.

(F) Time series of Casp3 and cPARP when the association rate of holoenzyme and procaspase 3 is decreased by 10% (broken lines). The results obtained under standard parameter are the same as in (A) and are shown to facilitate comparison. The insets in (A) and (D) show representative time courses of 1.5 h. The units of y axes in (A), (D), and (F) are nM. Abbreviation: aCalp, activated calpain; Holo, holoenzyme; Casp3, caspase 3.

As shown in Figure 3A, the transition from oscillatory to gradual pattern involves two changes. First, the oscillation amplitudes of the upstream species become successively smaller. In detail, it is about 3,000 nM for Ca^{2+}, nearly 3 nM for aCalp, only 0.03 nM for Bid and tBid, and barely perceptible for MOMP. To compare the oscillation strength among different species with a uniform standard, an oscillation coefficient, which is the ratio of oscillation amplitude to mean (looks like the deterministic version of the coefficient of variation), is calculated (Figure 3B). As a consequence, the oscillation coefficients of Ca^{2+} and aCalp are far larger than those of Bid, tBid, and MOMP. Here we define a signal as oscillatory if the oscillation coefficient of a species is larger than 0.1. Accordingly, the signals of Bid, tBid, and MOMP are not considered oscillatory. Second, upon stimulation, the system transitions from a resting steady state to a new equilibrium state, generating a transient time, which is defined as the time required for oscillatory species to reach steady oscillation or for other species to reach 90% of their peaks. As a result, the transient times for Ca^{2+}, aCalp, Bid, tBid, and MOMP are about 0.1, 0.5, 6, 6, and 12 h, respectively (Figure 3C), becoming successively longer. Compared with the length of cell cycle (18 h), a transient

time longer than 6 h is a duration that is not negligible. Therefore, we suggest that such a non-oscillatory signal with long transient time should be labeled as gradual. According to the oscillation coefficient and transient time, we therefore classify Ca^{2+} and aCalp as oscillatory signals and Bid, tBid, and MOMP as gradual signals.

Obviously the most dramatic change in the kinetics from Ca^{2+} to MOMP occurs upon the truncation of Bid by aCalp. The result of parameter sensitivity analysis also shows that this step indeed exerts a substantial influence on the output of the system (Figure S2B). Interestingly, the kinetics of Bid owns two distinct timescales. On the one hand, Bid oscillates at a fast timescale of around 200 s. On the other hand, a gradually decreasing trend occurs for Bid in a slower timescale of about 6 h as a transient process (Figure 3A). Meanwhile, the oscillation amplitude is far smaller than the mean value of its steady oscillations. This is mainly due to the slow truncation reaction of Bid by aCalp, which directly results in a long transient time and also generates a small oscillation amplitude for Bid by averaging aCalp over a long duration with slow association rate of aCalp with Bid (5×10^{-6} $nM^{-1}s^{-1}$). If this rate is increased 1,000-fold, Bid will achieve its new equilibrium very quickly and its oscillation coefficient will be 0.44 (Figure 3D), thus becoming an oscillatory signal. The slow truncation of Bid by aCalp, therefore, plays a significant role to convert the oscillatory signals to gradual signals in this pathway.

The kinetics from Bid to cPARP (Figure 3A) shows a transition from a gradual pattern to a switch-like pattern. Here, we distinguish a switch-like signal from gradual signal according to their switch time, which is defined as the time it takes to progress from a 30% to a 70% final concentration of any reaction species. If its switch time is longer than 2 h, it is labeled a gradual signal; otherwise, it is labeled a switch-like signal. According to this classification, Bid, tBid, MOMP, Cyt c, and holoenzyme are gradual signals, whereas caspase 3 and cPARP are switch-like signals (Figure 3E). If the switch time is defined as the time for a signal to increase from 20% to 80% of its final value, similar results are obtained, albeit with a longer switch time.

As a gradual signal, the MOMP-released Cyt c leads to a gradual accumulation of the apoptosome and thus the holoenzyme. In detail, before MOMP accumulates to reach a threshold, Cyt c cannot be released, thus maintaining Cyt c and downstream signals in an "off" state. After MOMP reaches the threshold at about 9 h (marked by asterisk in Figure 3A), the Cyt c-induced holoenzyme assembly ensures the downstream signals switch to an "on" state.

The conversion from gradual to switch-like signals is regulated by multiple reactions, including the mechanics of MOMP assembly, mitochondria-to-cytosol translocation of Smac and Cyt c (Albeck et al., 2008), the direct repression of holoenzyme and caspase 3 by XIAP (Figure S3), and holoenzyme-mediated activation of caspase 3. As seen in Figure 3A, holoenzyme activation results in a sudden and rapid cleavage of caspase 3 and thus the processing of PARP into cPARP, suggesting that the conversion from gradual to switch-like signals is strongly influenced by the interaction between holoenzyme and procaspase 3. If the association rate of holoenzyme and procaspase 3 (1.0 $\mu M^{-1}s^{-1}$) is decreased to 10%, the original switch-like signals, i.e., caspase 3 and cPARP, will become gradual signals (Figure 3F). Thus, the holoenzyme-mediated activation of caspase 3 has a crucial influence on the conversion from gradual into switch-like signals.

Three Ideal Ca^{2+} Inputs

Since both the amplitude and frequency of the ER-involved Ca^{2+} oscillations largely increase with stimulus strength (Figures 2B and 2C), it is hard to dissect the individual contributions of amplitude and frequency to apoptosis. To explore whether amplitude or frequency of Ca^{2+} oscillations is the critical determinant for Ca^{2+}-induced apoptosis, three ideal Ca^{2+} waveforms and their effects on the two indexes for evaluating apoptosis are presented in Figure 4.

First a constant Ca^{2+} input is imposed to assess its efficacy in triggering apoptosis. Figure 4A shows that, as the amplitude of the constant Ca^{2+} increases, the final [cPARP] exhibits an almost all-or-none pattern. When the amplitude increases beyond an apoptotic threshold, the apoptosis latency decreases first rapidly and then slowly approaches 5 h (Figure 4B). Different from the high amplitude threshold of 3 μM [Ca^{2+}] for apoptosis with an oscillatory Ca^{2+} signal, a small [Ca^{2+}] threshold of 1.5 μM is obtained with constant Ca^{2+} input for apoptosis. These results suggest that Ca^{2+} amplitude alone is sufficient to cause a low or high final [cPARP], corresponding to survival or apoptosis of cells.

Second, we used a square-wave Ca^{2+} input to investigate the roles of its amplitude and frequency in regulating apoptosis. For such a pulsating Ca^{2+} signal, besides the amplitude, we can define the wave width (T_w)

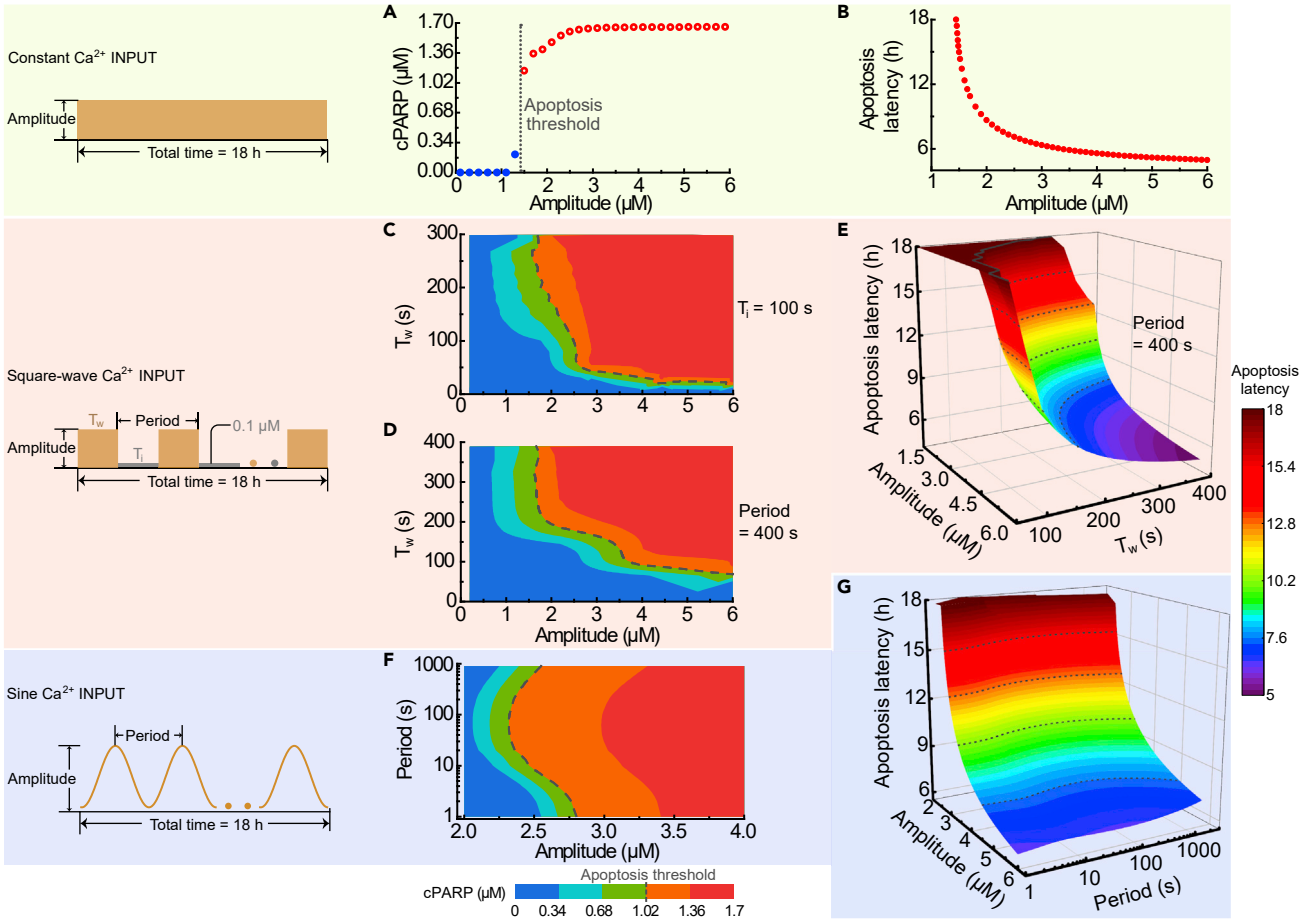

Figure 4. Three Ideal Ca^{2+} Inputs and Their Impact on Apoptosis

(A and B) The final [cPARP] (A) and apoptosis latency (B) as a function of the amplitude of constant Ca^{2+} input. (C) The final [cPARP] in response to the amplitude and period (varying T_w with the unchanged T_i) of square-wave Ca^{2+} input. (D and E) The final [cPARP] (D) and apoptosis latency (E) in response to the amplitude and T_w with the fixed period of square-wave Ca^{2+} input. (F and G) The dependence of the final [cPARP] (F) and apoptosis latency (G) on the amplitude and period of sinusoidal Ca^{2+} input. (C), (D), and (F) have the same color bar at the bottom, whereas (E) and (G) share the same color bar on the right.

and inter-wave interval (T_i), which can be varied separately, as well as the period (T_w + T_i). Such type of signal has been used experimentally (De Koninck and Schulman, 1998) and in mathematical models (Marhl et al., 2006; Salazar et al., 2008). In the case of varied wave width but fixed inter-wave interval, the contour map in Figure 4C shows that the final [cPARP] mainly depends on the Ca^{2+} amplitude but not on the wave width and of course not on its period. Figure 4D shows the dependence of final [cPARP] on the Ca^{2+} amplitude and wave width, while keeping the period constant. From the apoptosis threshold (dashed line) shown in Figure 4D, one can see that the final [cPARP] is high when the Ca^{2+} amplitude is large (>1.5 μM) and the wave width is long (>75 s). Thus, the Ca^{2+} amplitude is the dominant pro-apoptotic factor.

The comparison of the results in Figures 4C and 4D reveals that the final [cPARP] depends less on oscillation period than on its wave width. Next, we examined the influence of the Ca^{2+} amplitude and wave width on apoptosis latency. The result plotted in Figure 4E indicates that apoptosis latency is less sensitive to wave width than to wave amplitude. A similar but more obvious trend for apoptosis latency can be found when comparing Ca^{2+} amplitude and period (Figure S4). Together, the results obtained in Figures 4C–4E and S4 indicate that apoptosis is mainly modulated by amplitude, rather than frequency of a square-wave Ca^{2+} input.

Third we used sinusoidal Ca^{2+} input to further strengthen the conclusion that apoptosis depends more on amplitude than on frequency. The sinusoidal input mimics more closely biological Ca^{2+} oscillations, and its

oscillation amplitude and period can be varied separately. Figure 4F shows that the final [cPARP] exhibits only a modest response to the change of Ca^{2+} oscillation period but a pronounced sensitivity to the change of oscillation amplitude. Notably, a cell remains alive when its Ca^{2+} amplitude is small but undergoes apoptosis when the amplitude is large, regardless of the oscillation period. This result holds true when the top two most sensitive parameters are varied in a limited range (Figures S5). In addition, the change in Ca^{2+} amplitude significantly influences apoptosis latency, whereas its period does not (Figure 4G). These results reveal that AM is the dominant mechanism for Ca^{2+}-regulated apoptosis.

In summary, by virtue of three ideal Ca^{2+} waveforms, we demonstrated that cytosolic Ca^{2+} regulates apoptosis mainly via AM but not via FM. Although the Ca^{2+} amount or average Ca^{2+} and action time of Ca^{2+} input also have impacts on apoptosis (Figures S6 and S7), these factors appear insignificant.

Signal Transduction of Sinusoidal Ca^{2+} Input

Given that sinusoidal Ca^{2+} oscillations can mimic one of the two biologically oscillatory patterns (the sinusoid-like oscillations and the repetitive spikes) *in vivo* (Berridge, 1990; Putney and Bird, 1993), we explored the roles of amplitude and frequency of sinusoidal Ca^{2+} oscillations in the apoptotic signal transduction pathway. Figure 5A presents the temporal evolution of four key species in the signal transduction process where the Ca^{2+} amplitude is 2.5 μM and its period is 200 s. Here, aCalp is an oscillatory signal, tBid and holoenzyme are gradual signals, and cPARP is a switch-like signal, which are almost the same as those induced by the ER-involved Ca^{2+} oscillations (Figure 3A).

If the period of sinusoidal Ca^{2+} input becomes significantly shorter or longer, i.e., 50 s or 500 s, the kinetics of the four species change slightly (Figure 5B). The frequency information carried in Ca^{2+} oscillations becomes largely suppressed within the gradual signal of tBid. In contrast, if the amplitude of sinusoidal Ca^{2+} input becomes smaller or bigger, i.e., 2 or 3 μM, the kinetics of the four species change significantly, especially for the holoenzyme and cPARP (Figure 5C). A decreased amplitude causes the original switch-like cPARP signal to become a gradual signal, and the eventual cell fate changes from apoptosis to survival. An increased amplitude transforms the original gradual holoenzyme signal into a switch-like signal, and the apoptosis latency becomes dramatically shorter. The time course study suggests that the signal transduction from Ca^{2+} to tBid acts as a frequency filter of the Ca^{2+} oscillation information. Moreover, the information of the Ca^{2+} amplitude is important to determine the final intensity of the gradual signals, which is in turn crucial to determine the curve pattern of cPARP.

To gain further insights into these mechanisms, we analyzed how the changes in the period and amplitude of a sinusoidal Ca^{2+} input affect the oscillation coefficient, transient time, and switch time of the key species.

First, we considered the situation where the sinusoidal Ca^{2+} period changes from 10 to 1,000 s, while keeping the amplitude constant at 2.5 μM. Figure 5D depicts the change of the oscillation coefficients of aCalp and tBid, the transient times of MOMP and cPARP, and the switch times of caspase 3 and cPARP against the sinusoidal Ca^{2+} period. In order to clearly describe the process of information transformation, Figure S8A shows the distribution of the values of the three characteristic times of all key species. To accommodate the wide range of values, these values are normalized with respect to the corresponding value at period = 200 s, and each box plot in Figure 5E exhibits the distribution of the normalized values. Then, we considered the situation where the sinusoidal Ca^{2+} amplitude varies from 2 to 4 μM, while keeping the period constant at 200 s. Figures 5F, 5G, and S8B are the counterparts of Figures 5D, 5E, and S8A, respectively.

Figures 5D and 5F show that the oscillation coefficient of aCalp is far larger than that of tBid, which indicates that the frequency attribute of Ca^{2+} oscillations is only well retained in the aCalp signal, whereas it is largely lost in the gradual signals. When comparing Figures 5E and 5G, it is evident that the change in the period of a sinusoidal Ca^{2+} input only significantly affects the oscillation coefficients of the two upstream gradual signals, i.e., Bid and tBid, whereas the change in the Ca^{2+} amplitude dramatically modulates both the transient times and switch times of the downstream species, especially for the switch-like signals, i.e., caspase 3 and cPARP. Together, these results imply that the Ca^{2+}-regulated apoptotic transduction pathway is capable of efficiently filtering the frequency attribute during the transformation from oscillatory signals to gradual signals but capable of sensitively responding to the amplitude attribute of the Ca^{2+} oscillations.

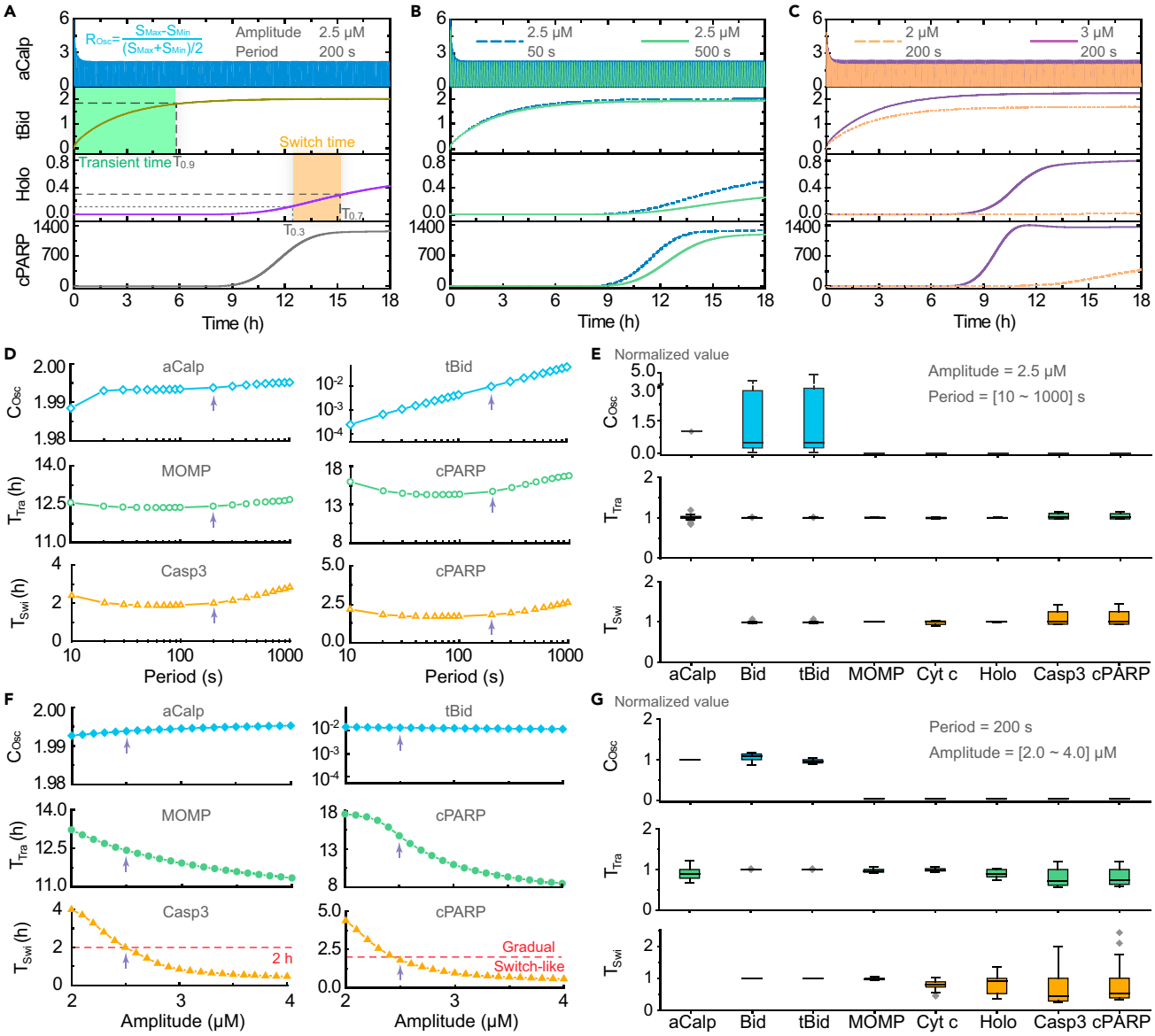

Figure 5. Effects of Amplitude and Period of Sinusoidal Ca^{2+} Input on Signal Transduction

(A-C) Time series of representative species such as aCalp, tBid, Holo, and cPARP (A) at amplitude = 2.5 μM and period = 200 s, (B) at amplitude = 2.5 μM and period = 50 s or 200 s, and (C) at period = 200 s and amplitude = 2 μM or 3 μM. The units of y axes are nM.

(D) Oscillation coefficient (C_{Osc}) of aCalp and tBid, transient time (T_{Tra}) of MOMP and cPARP, and switch time (T_{Swi}) of Casp3 and cPARP, keeping the amplitude constant at 2.5 μM and changing the period.

(E) C_{Osc}, T_{Tra}, and T_{Swi} of the main species are normalized to the corresponding value at amplitude = 2.5 μM and period = 200 s, as indicated by the arrows in (D).

(F and G) (F) and (G) are the counterparts of (D) and (E), respectively, but at fixed period of 200 s and varying amplitude. In the box plot, the middle line denotes the median; the top and bottom of the box denote 75th and 25th percentiles, respectively; whiskers denote 1.5×interquartile range; and diamonds denote outliers. Abbreviation: aCalp, activated calpain; Holo, holoenzyme; Casp3, caspase 3.

Hence, the results here reveal the underlying mechanism that Ca^{2+} signal regulates apoptosis mainly via the Ca^{2+} oscillation amplitude, rather than via its frequency.

DISCUSSION

Given the difficulties of experimentally tracking long-term Ca^{2+} signaling dynamics simultaneously with apoptotic protein processing, it is currently unknown how a fast and oscillatory Ca^{2+} signal transforms

into a slow but switch-like apoptotic response. How Ca^{2+} signaling regulates apoptosis has also remained elusive because the amplitude and period of Ca^{2+} oscillations cannot be manipulated independently within a biological system. We address these two fundamental questions with a mathematical model for deciphering the mechanism underlying Ca^{2+}-induced apoptosis.

Our results indicate that the conversion of an oscillatory Ca^{2+} signal into a switch-like apoptotic signal requires two steps. In the first step, oscillatory signals transform into gradual signals during which the oscillation amplitudes of the upstream species in signal cascade decrease successively, meanwhile their transient times to the new equilibrium increase successively. During this transformation, the slow truncation of Bid by aCalp plays a significant role. In the second step, gradual signals are converted into switch-like signals, during which the switch times of the downstream species in the apoptotic signaling pathway decrease dramatically. This process critically depends on the fast activation of caspase 3 by the holoenzyme.

Cellular information can be encoded in the amplitude and frequency of Ca^{2+} oscillations, and that information can then be decoded by distinct downstream effectors to achieve different cellular outcomes (Berridge, 1997; Monteith et al., 2017). The predominant view is that the cellular function is determined by the frequency of Ca^{2+} oscillations (Dupont and Combettes, 2016; Dupont and Sneyd, 2017; Goldbeter et al., 1990; Smedler and Uhlén, 2014). In contrast, our results show that the amplitude of Ca^{2+} oscillations is primarily used to modulate apoptosis in three different systems, that is, in the constant, square-wave, and sinusoidal Ca^{2+} input systems. Of note, the elucidation in the last system is compelling not only because sinusoidal Ca^{2+} input has separable amplitude and period but also because it can largely mimic the biologically oscillatory pattern observed in cells. Strikingly, by employing sinusoidal Ca^{2+} input, we revealed that the frequency property of Ca^{2+} oscillations is filtered but the amplitude property is retained during the apoptotic signal transduction process. During the process to translate these oscillatory signals into gradual signals, the oscillatory Ca^{2+} signal is converted into a non-oscillatory signal by filtering out the frequency information. Thus, the amplitude, other than the frequency, of Ca^{2+} oscillations, functions as the more important attribute for apoptosis induction.

The mechanisms by which cells encode the dynamic properties of oscillatory signaling (e.g., amplitude and/or frequency) into their decision-making processes are the subject of very intense investigation (Benzinger and Khammash, 2018; Cai et al., 2008; Hannanta-anan and Chow, 2016; Hansen and O'Shea, 2015). For a Ca^{2+} signal, it is generally believed that AM is less reliable than FM, owing to the difficulty of distinguishing small Ca^{2+} changes from the background noise level (Berridge et al., 1998). However, the fidelity of apoptotic Ca^{2+} signal can by guaranteed through AM mode because the apoptotic Ca^{2+} levels are much higher than those produced by spontaneous fluctuation. Indeed, a recent experiment revealed that individual cells exhibit high amplitude Ca^{2+} release events but significant heterogeneity in the frequency of these events after treatment with apoptosis-inducing drugs (Garcia et al., 2017). In addition, Monteith et al. recently proposed that it is the amplitude of Ca^{2+} oscillations that controls cell fate (e.g., proliferation or cell death), whereas it is their frequency that controls gene transcription (Monteith et al., 2017). Our finding demonstrates that Ca^{2+}-regulated apoptosis is a typical example of AM fashion, which is a key perspective in the field of Ca^{2+} signaling.

Limitations of the Study

Although Ca^{2+} oscillations are intrinsically stochastic because of stochastic IP_3R channel dynamics (Powell et al., 2020; Thul, 2014; Thurley et al., 2012), the Ca^{2+} oscillations at the cellular level can be effectively treated as deterministic (Cao et al., 2014; Sneyd et al., 2017; Voorsluijs et al., 2019). As a result, we only used the two-variable Li-Rinzel model as the simplest but useful model to produce Ca^{2+} oscillations. The focus of this work is on cytosolic Ca^{2+}-induced apoptosis, and for simplicity, we did not take mitochondrial Ca^{2+} into account. In addition, the prediction of AM given in the paper largely depends on a sinusoidal type of Ca^{2+} oscillations. Thus, whether our prediction can be generalized to other types of Ca^{2+} oscillations such as repetitive spikes remains an open question for future study. Furthermore, the test of this prediction will rely on the experimental design that can compare directly the effects of the amplitude and period of cytosolic Ca^{2+} oscillations on the apoptosis.

Resource Availability

Lead Contact

Jianwei Shuai

Materials Availability

This study did not generate new unique reagents.

Data and Code Availability

All data needed to evaluate the conclusions in the paper are present in the paper and/or the Supplemental Information. The code related to this paper may be requested from the authors.

Methods

All methods can be found in the accompanying Transparent Methods supplemental file.

SUPPLEMENTAL INFORMATION

Supplemental Information can be found online at https://doi.org/10.1016/j.isci.2020.101671.

ACKNOWLEDGMENTS

This work was supported by National Natural Science Foundation of China (Grants 11675134, 11874310, 11504214, 11704318, and 61873154), Shanxi Province Science Foundation for Youths (Grant 201901D211159), Scientific and Technological Innovation Programs of Higher Education Institutions in Shanxi (Grant 2019L0015), Natural Sciences and Engineering Research Council of Canada (Grant RGPIN-2015-04105)

AUTHOR CONTRIBUTIONS

H.Q. and J.S. designed research; H.Q. and X.L. performed research; X.L., Z.J., and T.S. analyzed data; H.Q., T.S., and J.S. wrote the paper.

DECLARATION OF INTERESTS

The authors declare no conflict of interest.

Received: March 11, 2020
Revised: August 15, 2020
Accepted: October 8, 2020
Published: November 20, 2020

REFERENCES

Albeck, J.G., Burke, J.M., Spencer, S.L., Lauffenburger, D.A., and Sorger, P.K. (2008). Modeling a snap-action, variable-delay switch controlling extrinsic cell death. PLoS Biol. *6*, e299.

Anderson, M.W., Moss, J.J., Szalai, R., and Lane, J.D. (2019). Mathematical modeling highlights the complex role of AKT in TRAIL-induced apoptosis of colorectal carcinoma cells. iScience *12*, 182–193.

Benzinger, D., and Khammash, M. (2018). Pulsatile inputs achieve tunable attenuation of gene expression variability and graded multi-gene regulation. Nat. Commun. *9*, 3521.

Berridge, M.J. (1990). Calcium oscillations. J. Biol. Chem. *265*, 9583–9586.

Berridge, M.J. (1997). The AM and FM of calcium signalling. Nature *386*, 759–760.

Berridge, M.J., Bootman, M.D., and Lipp, P. (1998). Calcium - a life and death signal. Nature *395*, 645–648.

Berridge, M.J., Bootman, M.D., and Roderick, H.L. (2003). Calcium signalling: dynamics, homeostasis and remodelling. Nat. Rev. Mol. Cell Biol. *4*, 517–529.

Boehning, D., Patterson, R.L., Sedaghat, L., Glebova, N.O., Kurosaki, T., and Snyder, S.H. (2003). Cytochrome c binds to inositol (1, 4, 5) trisphosphate receptors, amplifying calcium-dependent apoptosis. Nat. Cell Biol. *5*, 1051–1061.

Cai, L., Dalal, C.K., and Elowitz, M.B. (2008). Frequency-modulated nuclear localization bursts coordinate gene regulation. Nature *455*, 485–490.

Cao, P., Tan, X., Donovan, G., Sanderson, M.J., and Sneyd, J. (2014). A deterministic model predicts the properties of stochastic calcium oscillations in airway smooth muscle cells. PLoS Comput. Biol. *10*, e1003783.

Chen, M., He, H., Zhan, S., Krajewski, S., Reed, J.C., and Gottlieb, R.A. (2001). Bid is cleaved by calpain to an active fragment in vitro and during myocardial ischemia/reperfusion. J. Biol. Chem. *276*, 30724–30728.

Czabotar, P.E., Lessene, G., Strasser, A., and Adams, J.M. (2014). Control of apoptosis by the Bcl-2 protein family: implications for physiology and therapy. Nat. Rev. Mol. Cell Biol. *15*, 49–63.

Dupont, G., and Combettes, L. (2016). Fine tuning of cytosolic Ca^{2+} oscillations. F1000Res. *5*, 1–9.

Dupont, G., and Goldbeter, A. (1993). One-pool model for Ca^{2+} oscillations involving Ca^{2+} and inositol 1,4,5-trisphosphate as co-agonists for Ca^{2+} release. Cell Calcium *14*, 311–322.

Dupont, G., and Sneyd, J. (2017). Recent developments in models of calcium signalling. Curr. Opin. Syst. Biol. *3*, 15–22.

Garcia, M.I., Chen, J.J., and Boehning, D. (2017). Genetically encoded calcium indicators for studying long-term calcium dynamics during apoptosis. Cell Calcium *61*, 44–49.

Gerasimenko, J.V., Gerasimenko, O.V., Palejwala, A., Tepikin, A.V., Petersen, O.H., and Watson, A.J. (2002). Menadione-induced apoptosis: roles of cytosolic Ca^{2+} elevations and the mitochondrial permeability transition pore. J. Cell Sci. *115*, 485–497.

Giorgi, C., Marchi, S., and Pinton, P. (2018a). The machineries, regulation and cellular functions of

mitochondrial calcium. Nat. Rev. Mol. Cell Biol. *19*, 713–730.

Giorgi, C., Danese, A., Missiroli, S., Patergnani, S., and Pinton, P. (2018b). Calcium dynamics as a machine for decoding signals. Trends Cell Biol. *28*, 258–273.

Goldbeter, A., Dupont, G., and Berridge, M.J. (1990). Minimal model for signal-induced Ca^{2+} oscillations and for their frequency encoding through protein phosphorylation. Proc. Natl. Acad. Sci. U S A *87*, 1461–1465.

Hajnóczky, G., Robb-Gaspers, L.D., Seitz, M.B., and Thomas, A.P. (1995). Decoding of cytosolic calcium oscillations in the mitochondria. Cell *82*, 415–424.

Hanna, R.A., Campbell, R.L., and Davies, P.L. (2008). Calcium-bound structure of calpain and its mechanism of inhibition by calpastatin. Nature *456*, 409–412.

Hannanta-anan, P., and Chow, B.Y. (2016). Optogenetic control of calcium oscillation waveform defines NFAT as an integrator of calcium load. Cell Syst. *2*, 283–288.

Hansen, A.S., and O'Shea, E.K. (2015). Limits on information transduction through amplitude and frequency regulation of transcription factor activity. Elife *4*, e06559.

Jacob, R., Merritt, J.E., Hallam, T.J., and Rink, T.J. (1988). Repetitive spikes in cytoplasmic calcium evoked by histamine in human endothelial cells. Nature *335*, 40–45.

De Koninck, P., and Schulman, H. (1998). Sensitivity of CaM kinase II to the frequency of Ca^{2+} oscillations. Science *279*, 227–230.

Kupzig, S., Walker, S.A., and Cullen, P.J. (2005). The frequencies of calcium oscillations are optimized for efficient calcium-mediated activation of Ras and the ERK/MAPK cascade. Proc. Natl. Acad. Sci. U S A *102*, 7577–7582.

Lee, J.K., Lu, S., and Madhukar, A. (2010). Real-time dynamics of Ca^{2+}, caspase-3/7, and morphological changes in retinal ganglion cell apoptosis under elevated pressure. PloS one *5*, e13437.

Legewie, S., Blüthgen, N., and Herzel, H. (2006). Mathematical modeling identifies inhibitors of apoptosis as mediators of positive feedback and bistability. PLoS Comput. Biol. *2*, e120.

Li, Y.-X., and Rinzel, J. (1994). Equations for $InsP_3$ receptor-mediated $[Ca^{2+}]_i$ oscillations derived from a detailed kinetic model: a Hodgkin-Huxley like formalism. J. Theor. Biol. *166*, 461–473.

Li, W.-h., Llopis, J., Whitney, M., Zlokarnik, G., and Tsien, R.Y. (1998). Cell-permeant caged $InsP_3$ ester shows that Ca^{2+} spike frequency can optimize gene expression. Nature *392*, 936–941.

Li, Y., Zhou, M., Hu, Q., Bai, X.-c., Huang, W., Scheres, S.H., and Shi, Y. (2017). Mechanistic insights into caspase-9 activation by the structure of the apoptosome holoenzyme. Proc. Natl. Acad. Sci. U S A *114*, 1542–1547.

Marhl, M., Perc, M., and Schuster, S. (2006). A minimal model for decoding of time-limited Ca^{2+} oscillations. Biophys. Chem. *120*, 161–167.

Márquez-Jurado, S., Díaz-Colunga, J., Das Neves, R.P., Martinez-Lorente, A., Almazán, F., Guantes, R., and Iborra, F.J. (2018). Mitochondrial levels determine variability in cell death by modulating apoptotic gene expression. Nat. Commun. *9*, 389.

Monteith, G.R., Prevarskaya, N., and Roberts-Thomson, S.J. (2017). The calcium-cancer signalling nexus. Nat. Rev. Cancer *17*, 367–380.

Oancea, E., and Meyer, T. (1998). Protein kinase C as a molecular machine for decoding calcium and diacylglycerol signals. Cell *95*, 307–318.

Orrenius, S., Zhivotovsky, B., and Nicotera, P. (2003). Regulation of cell death: the calcium–apoptosis link. Nat. Rev. Mol. Cell Biol. *4*, 552–565.

Ow, Y.-L.P., Green, D.R., Hao, Z., and Mak, T.W. (2008). Cytochrome c: functions beyond respiration. Nat. Rev. Mol. Cell Biol. *9*, 532–542.

Parekh, A.B. (2011). Decoding cytosolic Ca^{2+} oscillations. Trends Biochem. Sci. *36*, 78–87.

Powell, J., Falcke, M., Skupin, A., Bellamy, T., Kypraios, T., and Thul, R. (2020). A statistical view on calcium oscillations. Adv. Exp. Med. Biol. *1131*, 799–826.

Putney, J.W., Jr., and Bird, G.S.J. (1993). The inositol phosphate-calcium signaling system in nonexcitable cells. Endocr. Rev. *14*, 610–631.

Qi, H., and Shuai, J. (2016). Alzheimer's disease via enhanced calcium signaling caused by the decrease of endoplasmic reticulum–mitochondrial distance. Med. Hypotheses *89*, 28–31.

Qi, H., Li, L., and Shuai, J. (2015). Optimal microdomain crosstalk between endoplasmic reticulum and mitochondria for Ca^{2+} oscillations. Sci. Rep. *2015*, 7984.

Qi, H., Jiang, Y., Yin, Z., Jiang, K., Li, L., and Shuai, J. (2018). Optimal pathways for the assembly of the Apaf-1·cytochrome c complex into apoptosome. Phys. Chem. Chem. Phys. *20*, 1964–1973.

Qiao, L., Zhao, W., Tang, C., Nie, Q., and Zhang, L. (2019). Network topologies that can achieve dual function of adaptation and noise attenuation. Cell Syst. *9*, 271–285.e7.

Rehm, M., Huber, H.J., Dussmann, H., and Prehn, J.H. (2006). Systems analysis of effector caspase activation and its control by X-linked inhibitor of apoptosis protein. EMBO J. *25*, 4338–4349.

Salazar, C., Politi, A.Z., and Höfer, T. (2008). Decoding of calcium oscillations by phosphorylation cycles: analytic results. Biophys. J. *94*, 1203–1215.

Santos, L.C., Vogel, R., Chipuk, J.E., Birtwistle, M.R., Stolovitzky, G., and Meyer, P. (2019). Mitochondrial origins of fractional control in regulated cell death. Nat. Commun. *10*, 1–10.

Scorrano, L., Oakes, S.A., Opferman, J.T., Cheng, E.H., Sorcinelli, M.D., Pozzan, T., and Korsmeyer, S.J. (2003). Bax and Bak regulation of endoplasmic reticulum Ca^{2+}: a control point for apoptosis. Science *300*, 135–139.

Shi, Y. (2004). Caspase activation: revisiting the induced proximity model. Cell *117*, 855–858.

Shuai, J., and Jung, P. (2003). Optimal ion channel clustering for intracellular calcium signaling. Proc. Natl. Acad. Sci. U S A *100*, 506–510.

Smedler, E., and Uhlén, P. (2014). Frequency decoding of calcium oscillations. Biochem. Biophys. Acta *1840*, 964–969.

Sneyd, J., Han, J.M., Wang, L., Chen, J., Yang, X., Tanimura, A., Sanderson, M.J., Kirk, V., and Yule, D.I. (2017). On the dynamical structure of calcium oscillations. Proc. Natl. Acad. Sci. U S A *114*, 1456–1461.

Spencer, S.L., and Sorger, P.K. (2011). Measuring and modeling apoptosis in single cells. Cell *144*, 926–939.

Spiller, D.G., Wood, C.D., Rand, D.A., and White, M.R.H. (2010). Measurement of single-cell dynamics. Nature *465*, 736–745.

Tait, S.W., and Green, D.R. (2010). Mitochondria and cell death: outer membrane permeabilization and beyond. Nat. Rev. Mol. Cell Biol. *11*, 621–632.

Thul, R. (2014). Translating intracellular calcium signaling into models. CSH Protoc. *2014*, 463–471.

Thurley, K., Skupin, A., Thul, R., and Falcke, M. (2012). Fundamental properties of Ca^{2+} signals. Biochem. Biophys. Acta *1820*, 1185–1194.

Uhlén, P., and Fritz, N. (2010). Biochemistry of calcium oscillations. Biochem. Bioph. Res. Commun. *396*, 28–32.

Voorsluijs, V., Dawson, S.P., De Decker, Y., and Dupont, G. (2019). Deterministic limit of intracellular calcium spikes. Phys. Rev. Lett. *122*, 088101.

Wang, H.-G., Pathan, N., Ethell, I.M., Krajewski, S., Yamaguchi, Y., Shibasaki, F., McKeon, F., Bobo, T., Franke, T.F., and Reed, J.C. (1999). Ca^{2+}-induced apoptosis through calcineurin dephosphorylation of BAD. Science *284*, 339–343.

Yao, J., Pilko, A., and Wollman, R. (2016). Distinct cellular states determine calcium signaling response. Mol. Syst. Biol. *12*, 894.

Yin, Z., Qi, H., Liu, L., and Jin, Z. (2017). The optimal regulation mode of Bcl-2 apoptotic switch revealed by bistability analysis. BioSystems *162*, 44–52.

Youle, R.J., and Strasser, A. (2008). The Bcl-2 protein family: opposing activities that mediate cell death. Nat. Rev. Mol. Cell Biol. *9*, 47–59.

Zhang, X.-P., Liu, F., and Wang, W. (2011). Two-phase dynamics of p53 in the DNA damage response. Proc. Natl. Acad. Sci. U S A *108*, 8990–8995.

Zhao, L., Sun, T., Pei, J., and Ouyang, Q. (2015). Mutation-induced protein interaction kinetics changes affect apoptotic network dynamic properties and facilitate oncogenesis. Proc. Natl. Acad. Sci. U S A *112*, E4046–E4054.

iScience, Volume *23*

Supplemental Information

The Oscillation Amplitude, Not the Frequency of Cytosolic Calcium, Regulates Apoptosis Induction

Hong Qi, Xiang Li, Zhen Jin, Thomas Simmen, and Jianwei Shuai

Supplementary Information

The Oscillation Amplitude, Not the Frequency of Cytosolic Calcium Regulates Apoptosis Induction

Hong Qi, Xiang Li, Zhen Jin, Thomas Simmen, and Jianwei Shuai

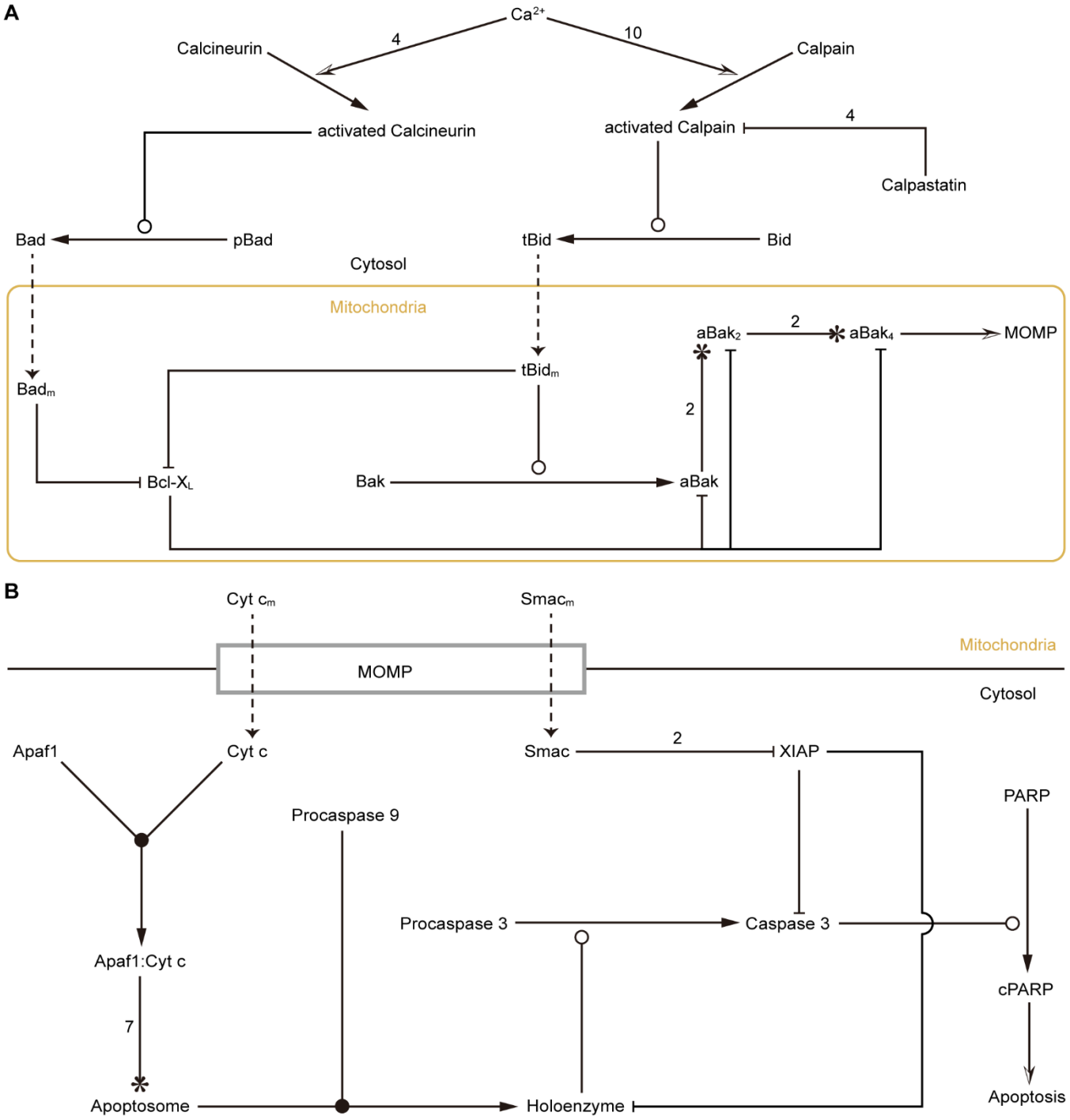

Figure S1. The detailed scheme of the last three modules, related to Figure 1. (A) Module of Ca^{2+}-activated proteins (top) and MOMP controlled by Bcl-2 protein family (bottom). (B) Module of Cyt c-induced caspase cascade. The graphical notations are the same as in Figure 1. The numbers beside the arrows refer to the stoichiometric number of the corresponding reaction.

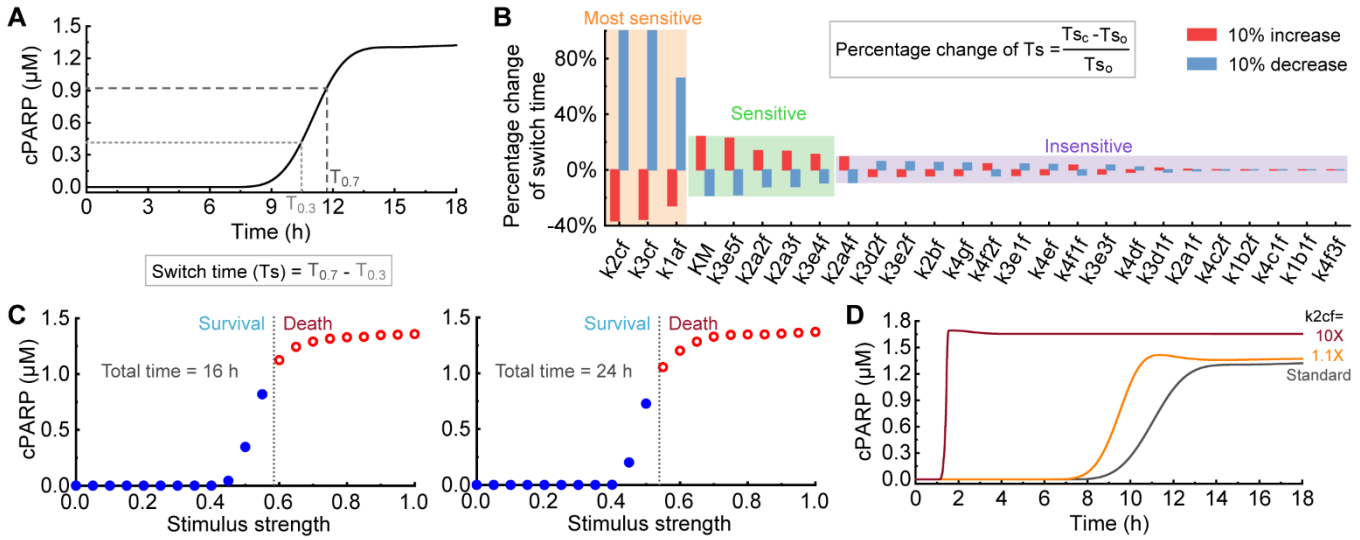

Figure S2. Parameter sensitivity analysis, related to Figures 2 and 3. (A) Illustration of the definition of switch time (T_{swi}, the time for cPARP to increase from 30 to 70% of its final concentration). (B) Percentage change of the switch time in response to 10% increase or decrease of each parameter. T0 is the switch time obtained under standard parameter conditions, and Tc is the one under changed parameter settings. See Table S3 for details of the meanings of parameters. (C) The final [cPARP] at different stimulus strengths when the total simulation time is 16 h (left) and 24 h (right), respectively. The dotted lines depict the apoptosis threshold. (D) Time series of cPARP when the association rate of aCalp and Bid (k_{2cf}) is increased by 10% and 10-fold. Stimulus strength=0.73.

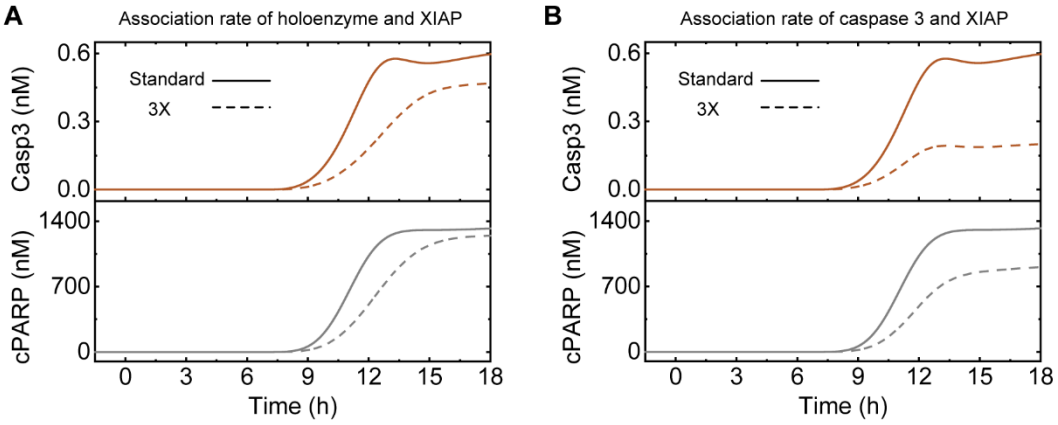

Figure S3. Influence of repression of holoenzyme and caspase 3 by XIAP on signal conversion, related to Figure 3. Time series of Casp3 and cPARP when the association rate of holoenzyme (or caspase 3) and XIAP is increased to 3-fold (broken lines).The curves obtained by the standard parameter value are shown in solid lines. Casp3, caspase 3.

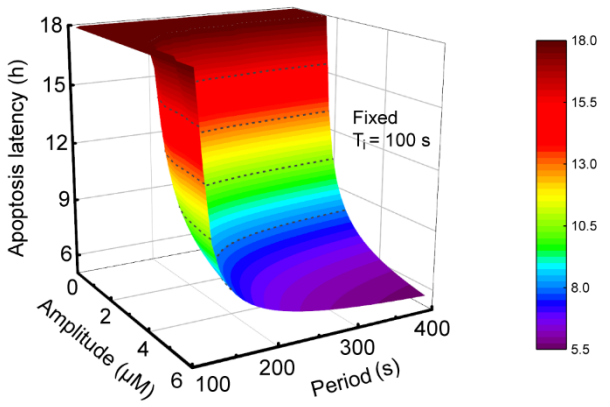

Figure S4. Apoptosis latency mainly depends on Ca^{2+} amplitude, but not on the period of square-wave Ca^{2+} input, related to Figure 4. The apoptosis latency in response to the amplitude and period with the fixed inter-wave interval (T_i) of square-wave Ca^{2+} input.

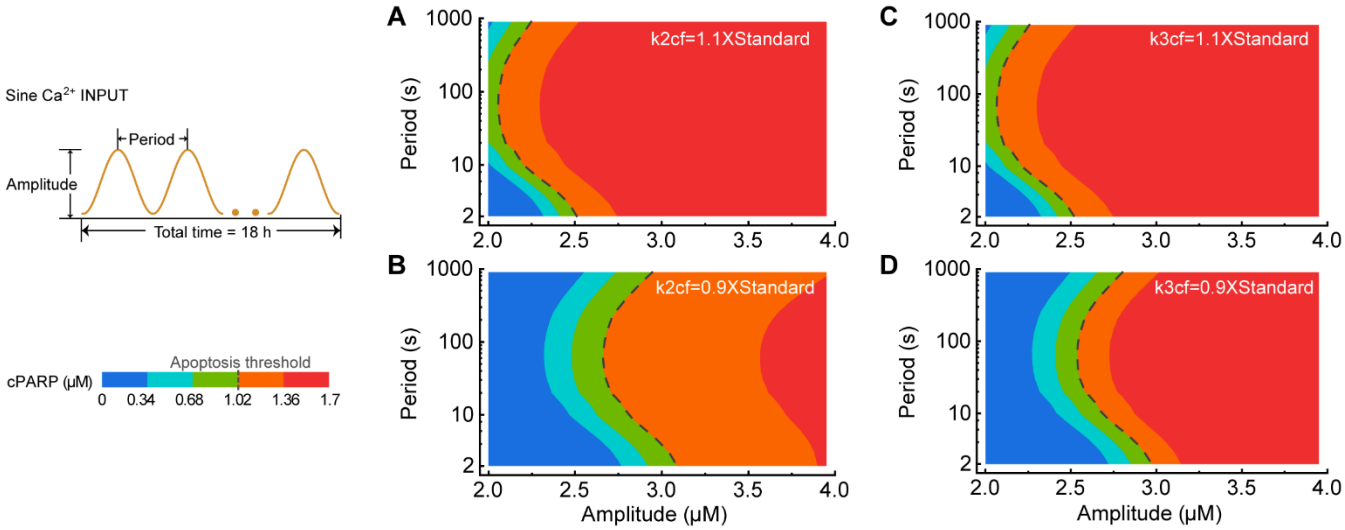

Figure S5. The robustness of the conclusion that Ca^{2+} regulates apoptosis mainly via AM, but not via FM, related to Figures 4 and S2. The final [cPARP] in response to the amplitude and period of sinusoidal Ca^{2+} input when the two most sensitive parameters, k_{2cf} and k_{3cf}, are varied ±10%.

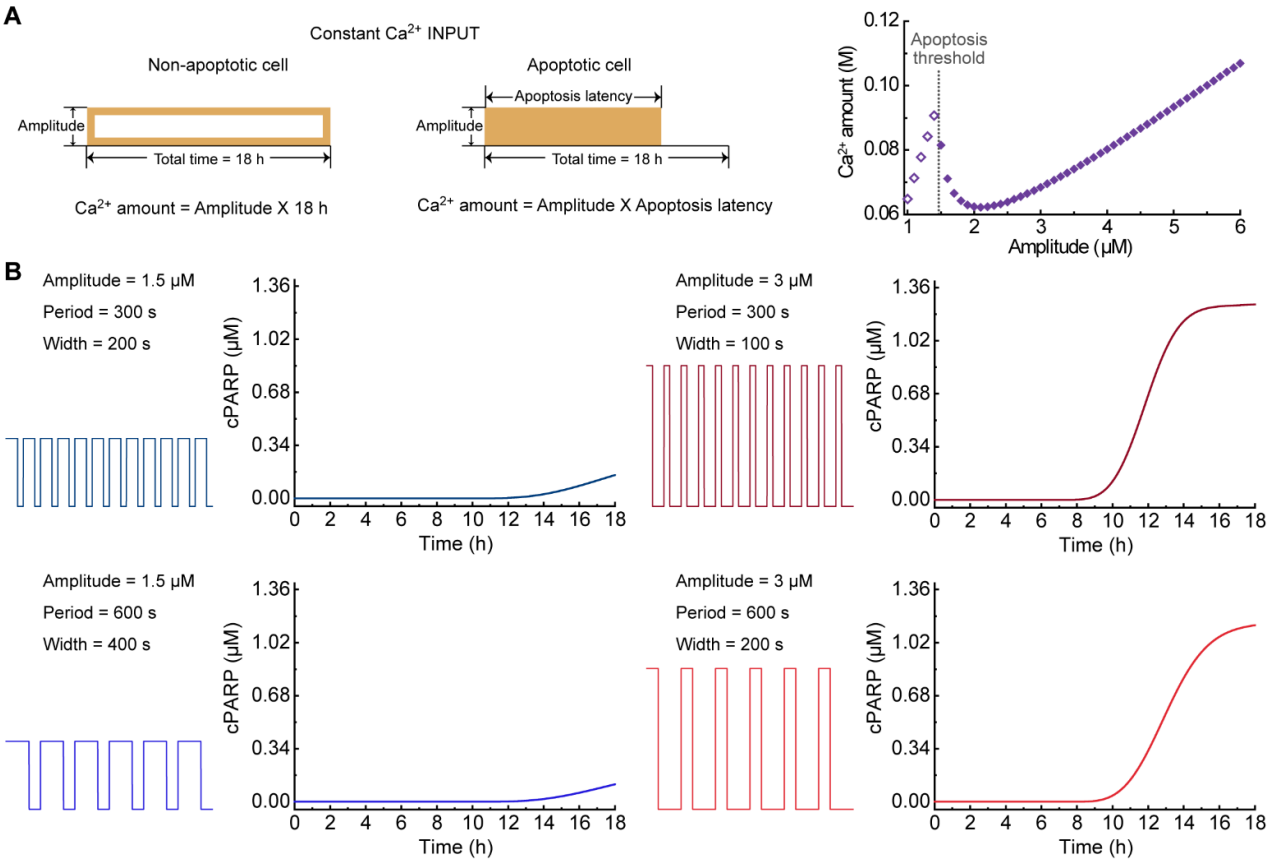

Figure S6. Effect of Ca^{2+} amount or average Ca^{2+} on the apoptosis, related to Figure 4. (A) Ca^{2+} amount as a function of the amplitude of constant Ca^{2+} input. Survival and death are corresponding to the left and right region of the apoptosis threshold, respectively. (B) The time series of [cPARP] with different square-wave Ca^{2+} input. Despite the waveforms of the Ca^{2+} input are different, their total Ca^{2+} amounts per hour (and thus the average Ca^{2+}) are identical.

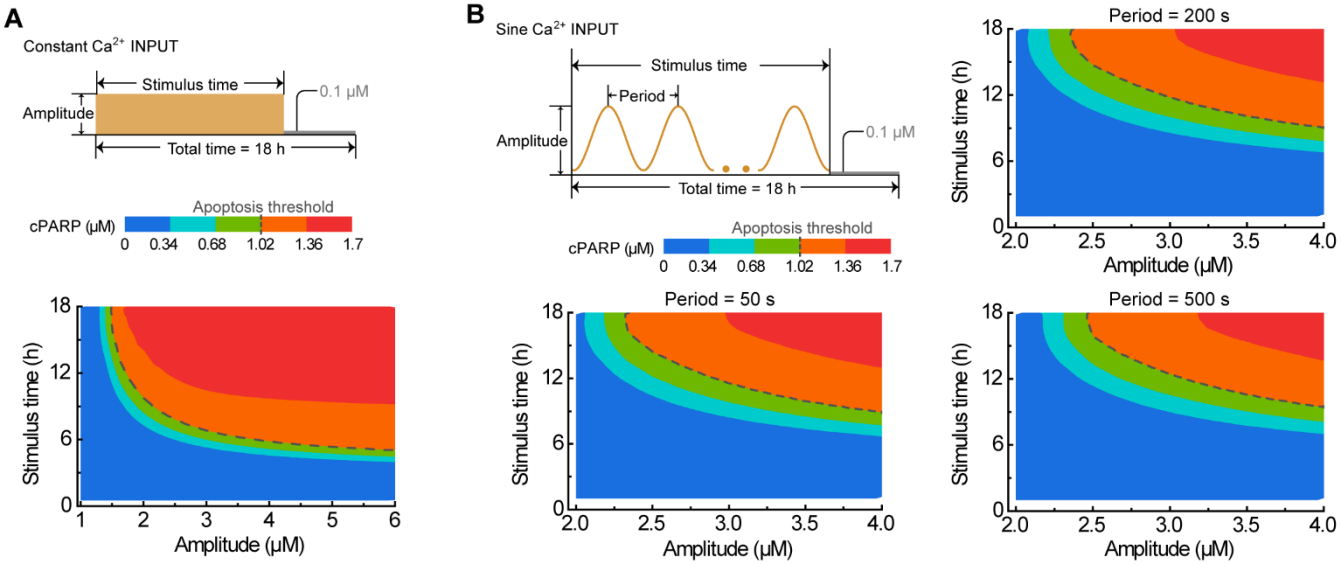

Figure S7. Effect of stimulus time on the apoptosis, related to Figure 4. (A) Dependence of the final [cPARP] on independent amplitude and stimulus time with constant Ca^{2+} input. (B) Under sinusoidal Ca^{2+} input, the final [cPARP] in response to the amplitude and stimulus time with fixed period of 50 s, 200 s, and 500 s, respectively.

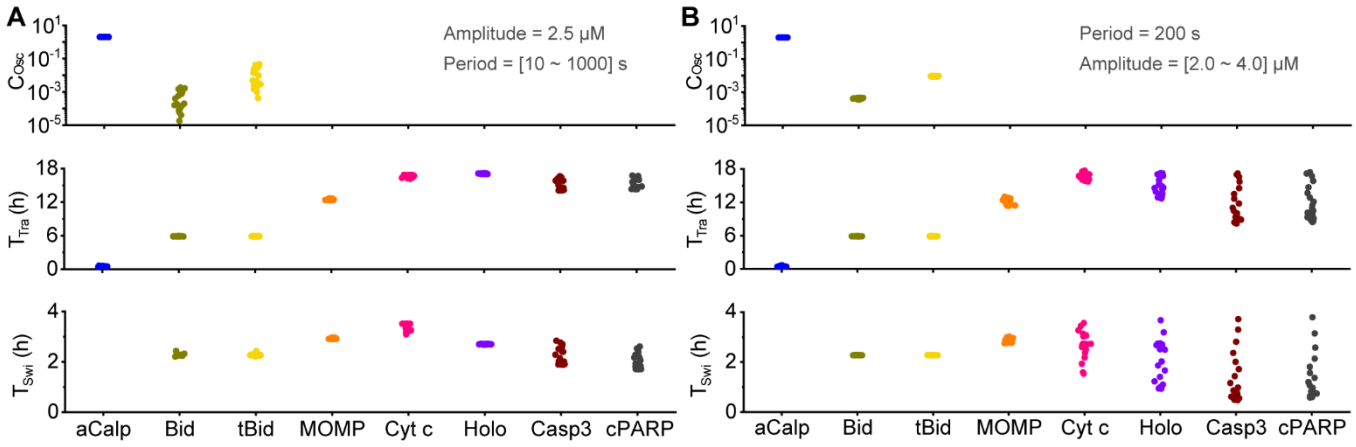

Figure S8. Distribution of three characteristic times, related to Figure 5. (A) Oscillation coefficient (C_{Osc}), transient time (T_{Tra}), and switch time (T_{Swi}) of the main species in the signaling pathway, keeping the amplitude constant at 2.5 μM and changing the period from 10 to 1000 s. (B) C_{Osc}, T_{Tra}, and T_{Swi} of the main species in the signaling pathway, keeping the period constant at 200 s and changing the amplitude from 2 to 4 μM.

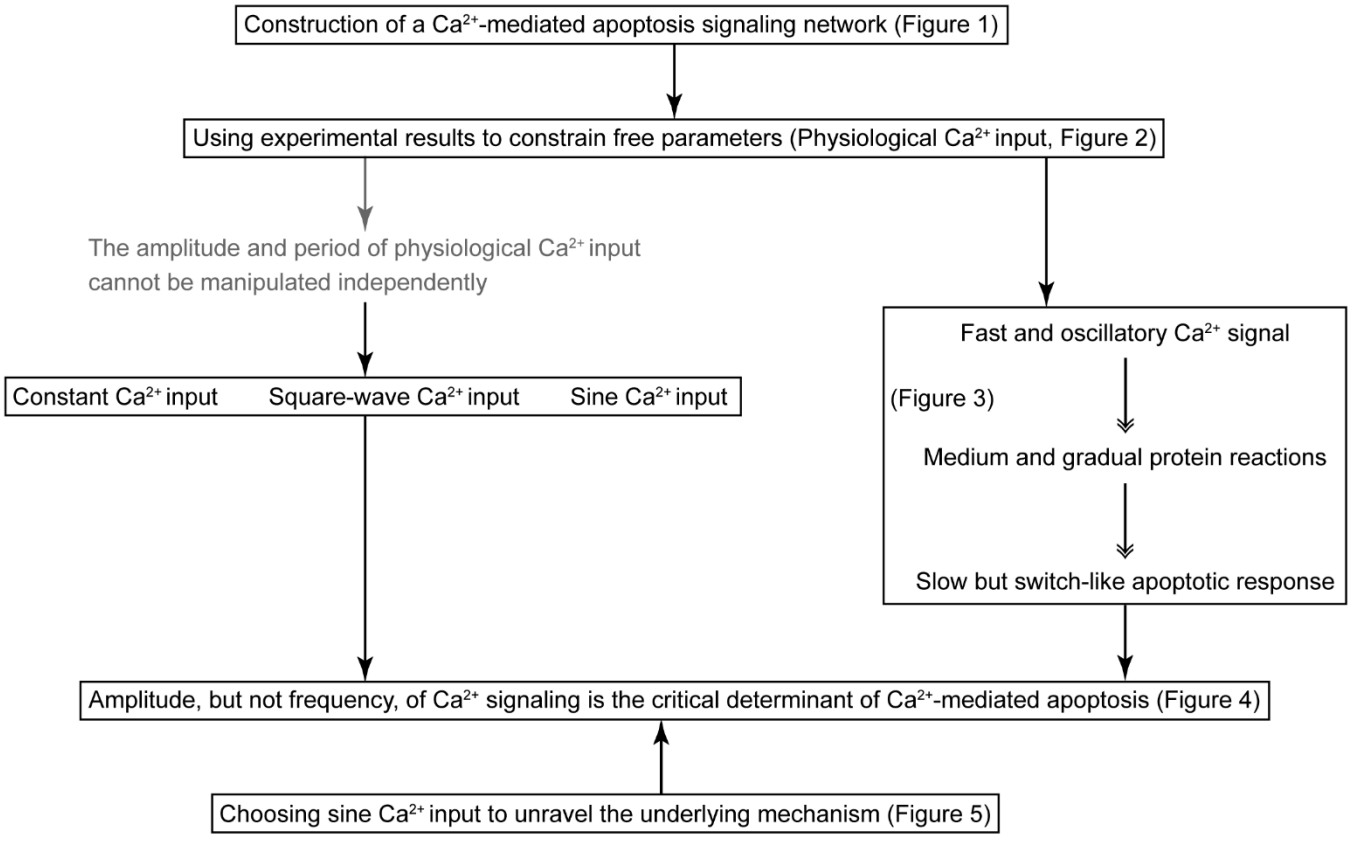

Figure S9. Workflow of the present work, related to Figures 1-5.

Transparent Methods

Detailed description of the model

In vertebrates, apoptosis typically proceeds through two main pathways: the extrinsic pathway and the intrinsic pathway. We primarily focus our attention on the latter due to the importance of cytosolic Ca^{2+} in the regulation of the intrinsic pathway (Harr and Distelhorst, 2010). To qualitatively study this process, we constructed a model comprised of four functional modules (Figure 1 and Figure S1), which are described in detail in following.

i. ER-involved Ca^{2+} oscillations

Under resting conditions, cytosolic Ca^{2+} concentration ($[Ca^{2+}]$) is maintained at low levels, while $[Ca^{2+}]$ in the endoplasmic reticulum (ER) is very high. Their homeostasis is dynamically regulated by active Ca^{2+} uptake through sarco/endoplasmic reticulum Ca^{2+}-ATPase (SERCA) and passive Ca^{2+} leak from the ER (Chang et al., 2014). Upon stress stimuli, IP_3 (inositol 1,4,5-trisphosphate) forms and binds to IP_3 receptors (IP_3Rs) to release Ca^{2+} from the ER, producing the upstroke of a Ca^{2+} oscillation. The SERCA then pumps the cytosolic Ca^{2+} back into the ER, completing the Ca^{2+} oscillation.

The Ca^{2+} oscillation module (blue region of Figure 1) is described by the two-variable Li-Rinzel model, which is simple but has a significant ability to reproduce experimental observations. In contrast to the original model (De Pitta et al., 2008), we made two modifications: a. for correlating the different stimulus strengths with different levels of IP_3, the production and degradation of IP_3 are considered additionally; b. the amplitude and period of Ca^{2+} oscillations are rescaled with the modified model parameters to better fit the Ca^{2+} oscillation patterns observed in experiment (Giorgi et al., 2018; Scorrano et al., 2003).

ii. Ca^{2+}-activated proteins

An important machinery linking cytosolic Ca^{2+} and apoptosis is the activation of two Ca^{2+}-regulated enzymes, calpain and calcineurin. The key mechanism for guarding against inappropriate activation of the two proteases is their weak affinity for Ca^{2+}. Calpain and calcineurin are activated by tens-of-micromolar and micromolar concentrations of Ca^{2+}, respectively.

Calcineurin has four Ca^{2+} binding sites: sites 1 and 2 with dissociation constants in the micromolar range, whereas sites 3 and 4 with dissociation constants in the nanomolar range (Li et al., 2011). Fully activated calpain needs to bind ten Ca^{2+} ions (Moldoveanu et al., 2008), but the activation mechanisms remain poorly

understood (Campbell and Davies, 2012). Here we made three simplifications and assumptions: a. Ca^{2+} ions bind calpain one by one; b. all binding sites have the same dissociation constant for Ca^{2+}; c. calpain is activated because of its vicinity to microdomains of high $[Ca^{2+}]$ ($[Ca^{2+}]_{Mic}$) (Hanna et al., 2007), which is 5- to 10-fold higher than in the bulk cytosol (Giacomello et al., 2010). For simplicity, we assumed that $[Ca^{2+}]_{Mic}$ is 7.5-fold higher than cytosolic $[Ca^{2+}]$ ($[Ca^{2+}]_{Cyt}$), the latter being determined by the modified Li-Rinzel model mentioned above. Calpastatin, an endogenous inhibitor of calpain, is capable of neutralizing four molecules of activated calpain (Hanna et al., 2008; Moldoveanu et al., 2008).

iii. MOMP controlled by Bcl-2 protein family

The activated calcineurin dephosphorylates the phosphorylated Bad into Bad (Wang et al., 1999). Activated calpain cleaves Bid into truncated Bid, tBid (Chen et al., 2001). Both Bad and tBid then migrate into the mitochondria and mediate mitochondrial outer membrane permeabilization (MOMP). In detail, tBid on the mitochondria directly activates Bak. Active Bak (aBak) monomers first form dimers and then tetramers, causing MOMP. Bcl-X_L is able to bind and antagonize all the active forms of Bak. Bad and tBid on the mitochondria can both bind to Bcl-X_L and release active forms of Bak to promote MOMP.

iv. Cyt c-induced caspase cascade

Following MOMP, mitochondrial intermembrane space proteins such as cytochrome c (Cyt c) and second mitochondria-derived activator of caspases (Smac) are released into the cytosol. In the cytosol, Cyt c engages apoptotic protease-activating factor-1 (Apaf1), and together form the heptameric apoptosome, which interacts with procaspase 9 to induce the formation of holoenzyme, thereby triggering caspase 3 activation. Caspase 3 in turn cleaves a series of substrates, including PARP, and ultimately leads to apoptosis. Smac facilitates apoptosis by neutralizing the holoenzyme and caspase inhibitor X-linked inhibitor of apoptosis protein (XIAP).

We used the mathematical model of apoptosis from (Albeck et al., 2008b) and (Rehm et al., 2006) as a template to construct the biochemical reactions of the last two modules, but two modifications have been made in our model. Since MOMP is a pore, and thus the drive force for the release of Cyt c and Smac via the MOMP is the concentration difference between two compartments (i.e., intermembrane space of mitochondria and cytosol). In the model we used a Hill function to model the release kinetics of Cyt c and Smac through the MOMP. In addition, our recent study proposed that there are 2047 pathways for the assembly of apoptosome (Qi et al., 2018). To avoid combinatorial complexity, we chose an optimal pathway in the current model.

Limitation of the model

The main purpose of the paper is to explore which characteristic of cytosolic Ca^{2+} oscillations regulates apoptosis, so three simplifications were made to reduce complexity of the problem without significantly affecting our result. First, although Ca^{2+} oscillations are mainly from the periodic release of Ca^{2+} within the ER in many cell types, the ER-to-mitochondria Ca^{2+} transfer, the mitochondria-to-cytosol Ca^{2+} transport and the Ca^{2+} exchange through the plasma membrane also impact Ca^{2+} oscillations. However, they are not considered in the current model. Second, it should be noted that mitochondria can sequester cytosolic Ca^{2+} and excessive Ca^{2+} accumulation within mitochondria causes the opening of mitochondrial permeability transition pore in the inner mitochondrial membrane, which results in increased mitochondrial permeability to ions and solutes, followed by organelle swelling and the rupture of the outer mitochondrial membrane, and thus the release of Cyt c, leading to apoptosis. Obviously, the consideration of mitochondrial Ca^{2+} in our model will make the situation very complex and therefore it has not been considered. Third, there may be complicated pathways for the long-duration Ca^{2+} oscillations to induce apoptosis. The long-duration Ca^{2+} oscillations may cause other sources of stress or lead to the transformation of Ca^{2+} oscillations into a sustained Ca^{2+} response to finally induce apoptosis. With a mathematic model, we are not trying to discuss various possible mechanisms of long-duration Ca^{2+} oscillations induced apoptosis, which can make the results simpler to interpret.

Rationality of parameter selection

In our model, the output of the Ca^{2+}-induced apoptosis system is regarded as cPARP, a switch-like signal. Accordingly, we performed parameter sensitivity analysis for 26 key parameters to identify their influence on the switch time of cPARP (Figure S2B). On each trial only one parameter is increased or decreased by 10% with respect to its standard value, while the others remain at their standard values. According to the result of k-means clustering, if the percentage change of the corresponding switch time is smaller than 10%, it is classified as an insensitive parameter, otherwise it is classified as a sensitive parameter; and if the percentage change is larger than 20%, it is regarded as a most sensitive parameter.

Approximately 70% of the parameters are insensitive, which are mostly related to the two downstream modules, i.e., MOMP controlled by Bcl-2 protein family and Cyt c-induced caspase cascade. The three most sensitive parameters are associated with the upstream reactions of signaling network, i.e., activation of calpain by Ca^{2+}, cleavage of Bid into tBid by aCalp, and tBid-mediated activation of Bak. The considerable influence of k_{2cf} (the association rate of aCalp and Bid) on the switch-like response suggests that it is the rate-limiting step in the signal transduction.

Giorgi et al. summarized that under resting conditions [Ca^{2+}] is maintained at about 0.1 μM, while after stimulation it can reach 0.2~5 μM (Giorgi et al., 2018). Although the critical [Ca^{2+}] threshold for apoptosis depends on the cell type and apoptotic stimuli, we must select a fixed one for the deterministic model to evaluate its correlation with the cell fate. Viewed in this perspective, we chose 3 μM [Ca^{2+}] as a critical threshold to initiate apoptosis. Similarly, Rehm et al. found that 25% substrate cleavage does not elicit apoptosis, while cells that exhibits 65% substrate cleavage undergo apoptosis (Rehm et al., 2006). Since the total [PARP] is 1.7 μM, we chose 60% substrate cleavage, i.e. 1.02 μM [cPARP] as a critical threshold to initiate apoptosis. As seen in Figure 2 in the main text, a stimulus strength of 0.6 promotes the peak of [Ca^{2+}] above 3 μM, which in turn results in [cPARP] more than 1.02 μM, inducing apoptotic cell death. We should stress that although choosing these two critical values is to some extent arbitrary, the current model is only qualitative, and thus these precise values in the model have little qualitative influence on the conclusion. Likewise, the conclusion is also robust to the detailed selection of the cell cycle, i.e. total simulation time (Figure S2C, compared to Figure 2E).

In addition, cells exposed to the same apoptotic stimulus always have different apoptosis latency. This is due to the intrinsic and extrinsic noise existed in the cells (Flusberg and Sorger, 2015), which can be reflected by variations of the parameter values of the model. Here we used k_{2cf} as an example to illustrate how its variation can influence the apoptosis latency (Figure S2D). If k_{2cf} is increased by 10%, the apoptosis latency is less than 8 h; and if k_{2cf} is increased by 10-fold, it becomes less than 2 h.

Influence of repression of holoenzyme and caspase 3 by XIAP on signal conversion

If the association rate of holoenzyme and XIAP is increased to 3-fold, the original switch-like signals, i.e. caspase 3 and cPARP, will become gradual signals (Figure S3A). If the association rate of caspase 3 and XIAP is increased to 3-fold, caspase 3 and cPARP will become lower (Figure S3B).

Apoptosis latency in response to amplitude and period of square-wave Ca^{2+} input

For the square-wave Ca^{2+} input, if the wave width is varied with the inter-wave interval fixed, the period of Ca^{2+} input varies with the wave width. The contour map in Figure S4 displays that apoptosis latency is significantly sensitive to wave amplitude, but slightly to period. This result indicates that the apoptosis latency is mainly dependent on the Ca^{2+} amplitude, but not on its period.

Apoptosis is not dependent on the Ca^{2+} amount or average Ca^{2+}

A recent study found a strategy called signal integration in the decision-making system for cell cycle (Liu et

al., 2015). To determine whether apoptosis is primarily a result of an integrator of cumulative Ca^{2+} load, we assess the amount of Ca^{2+} over 18 h to see whether apoptosis only occurs when Ca^{2+} amount reaches a certain threshold by imposing constant Ca^{2+} input. In detail, if the cell is still survival at the end of 18 h, the Ca^{2+} amount is equal to the total amount during the past 18 h. However, if the cell becomes death within 18 h, the Ca^{2+} amount is defined as the total amount accumulated in the period of apoptosis latency. From Figure 4A in the main text we can see that a plot of the final [cPARP] versus Ca^{2+} amplitude shows a monotonic relationship. In detail, the final [cPARP] is low if the Ca^{2+} amplitude is smaller than a threshold amplitude of 1.5 μM, while it is high if the Ca^{2+} amplitude is greater than the threshold amplitude. However, the amounts of Ca^{2+} around this threshold amplitude display a peak (Figure S6A). This clearly excludes the possibility of signal integration in our Ca^{2+}-apoptosis system.

Average Ca^{2+} maybe another factor to influence the apoptosis. We designed four different square-wave Ca^{2+} inputs: they have different amplitudes, periods, or wave widths, albeit with the same average Ca^{2+} level, i.e. 1 μM/s. The results in Figure S6B show that despite that period and wave width have a certain effect on the outcome (the final [cPARP]), amplitude is still the dominant factor. This demonstrates that Ca^{2+} amplitude is important even for a fixed average Ca^{2+}.

Effect of Ca^{2+} action time on the apoptosis

We need to point out that the stimulating duration of high Ca^{2+} signal may not be always 18 h in the apoptosis process. An experiment revealed that the Ca^{2+} release events last more than 10 h (Garcia et al., 2017). In addition, Ca^{2+} ions not only stimulate proapoptotic pathways, but also activate prosurvival pathways, and so cell fate is decided by the balance between survival and apoptotic pathways. We thus chose 18 h, i.e., the length of cell cycle, as the stimulus time in our standard procedure. Next we explored the model dynamics with constant and sinusoidal Ca^{2+} input to verify the robustness of our conclusions under the condition of varying stimulus time.

Constant Ca^{2+} input is the simplest input and is easy to illustrate the effect of stimulus time on cell fate. Here the total running time is still 18 h. As illustrated in Figure S7A, a high constant [Ca^{2+}] is added as a stimulus for a certain stimulus time, after which [Ca^{2+}] is set to 0.1 μM. The corresponding result indicates that a stimulus time of 6 h is enough to cause apoptosis, presumably as the minimal response time for the Ca^{2+}-induced apoptotic cascade in our model.

Sinusoidal Ca^{2+} input is employed to demonstrate that it is not the frequency of the Ca^{2+} oscillations, but

rather the amplitude, that dominates the extent of apoptotic response. In Figure S7B the abilities to induce apoptosis for Ca^{2+} inputs that have fixed period but with distinct amplitudes are compared. It is shown that apoptosis can be induced only when the stimulus time is longer than 9 h, depending mainly on the Ca^{2+} amplitude. Even though the periods of Ca^{2+} input are different, the response patterns of apoptosis to Ca^{2+} amplitude are similar. As a result, the conclusion that apoptosis acts primarily as a Ca^{2+} amplitude-selective, rather than a Ca^{2+} frequency-selective decoder, is not critically dependent on the duration of stimulus time.

Parameters, biochemical reactions, and ordinary differential equations

The principles of parameter selection are detailed in following paragraphs. The parameters of Ca^{2+} dynamics module, protein synthesis and degradation rates, and the kinetic rate parameters of other three modules, are summarized in Table S1, S2, and S3, respectively. Biochemical reactions and corresponding reaction rates are given in Table S4, and the resulting ordinary differential equations are listed in Table S5.

i. Choice of model parameters

Parameter selection is based on the following criteria:

a. Parameters are preferentially taken from the combined experimental and theoretical studies, then from experimental studies, and lastly from the preceding modeling studies.

b. Although measuring the cellular kinetic parameters is extremely difficult, most of the dissociation constants can be obtained from the literatures. So we can estimate the association rate constant by fixing the dissociation rate constant.

c. The unknown parameters are determined mainly by fitting the dynamics of Ca^{2+} and cPARP to the experimental measurements.

ii. Geometric parameters

The diameter of human cell is in the range of 5~100 μm (Ginzberg et al., 2015). Here we assumed that the cell is a sphere of radius 10 μm, giving the cell volume about 4190 μm^3. Given the mean mitochondrial volume is 0.5 μm^3 (Morigi et al., 2015) and each cell contains hundreds of mitochondria, we estimated the total mitochondrial volume of a cell is about 300 μm^3. So the cytosolic volume is 3890 μm^3, and the mitochondria-to-cytosol volume ratio is 0.077. If we assume that the mitochondrial intermembrane space occupies 10% of the mitochondrial volume, then the intermembrane space-to-cytosol volume ratio is 0.0077. The ER-to-cytosol volume ratio is assumed to be 0.185, which indicates that the ER accounts for approximately 15% of the total cell volume.

iii. Protein synthesis and degradation rate

Because we consider the dynamical behavior of the system within 18 h, the synthesis and degradation of proteins must be included. To reduce the number of free parameters, we assumed the same protein degradation rate for all molecular species, a procedure that was used in (Zhao et al., 2015). The only exception is the complex between XIAP and caspase 3. This is because XIAP-mediated degradation of caspase 3 is involved in restraining caspase 3 catalytic activity (Albeck et al., 2008a), and we consider an additional degradation rate for this complex. Protein synthesis rate can be obtained by the product of degradation rate and steady-state concentration of a certain protein.

Since Ca^{2+} is not created or destroyed or converted into an inactive metabolite (Monteith et al., 2017), in addition to the Ca^{2+} flux between the ER and cytosol, $[Ca^{2+}]$ in the cytosol changes only due to the association and dissociation reactions between Ca^{2+} and Ca^{2+}-binding proteins. When Ca^{2+}-binding proteins are degraded, the Ca^{2+} ions that bind with them release into the cytosol.

Table S1. Parameters in the Ca^{2+} dynamics module, related to Figure 1.

Parameter	Description	Value (Unit)	Reference[1]
C_0	Total [Ca^{2+}] in terms of cytosolic volume	9.4 (μM)	Rescaled
c_1	ER-to-cytosol volume ratio	0.185	(De Pitta et al., 2008)
v_1	Maximum IP_3R channel flux	0.4286 (s^{-1})	Rescaled
v_2	Ca^{2+} leak flux constant	0.0078 (s^{-1})	Rescaled
v_3	Maximum SERCA pump rate	0.151 (μM s^{-1})	Rescaled
K_3	Activation constant for SERCA	0.235 (μM)	Rescaled
d_1	IP_3R dissociation constant for IP_3 sites A	0.13 (μM)	(De Pitta et al., 2008)
d_2	IP_3R dissociation constant for Ca^{2+}-inhibition sites	2.4651 (μM)	Rescaled
d_3	IP_3R dissociation constant for IP_3 sites B	0.9434 (μM)	(De Pitta et al., 2008)
d_5	IP_3R dissociation constant for Ca^{2+}-activation sites	0.47 (μM)	Rescaled
a_2	IP_3R binding rate constant for Ca^{2+}-inhibition sites	0.006 (μM^{-1} s^{-1})	Rescaled
p_{IP3}	Maximum IP_3 synthesis rate	0.18 (μM s^{-1})	Adjusted
k_{IP3}	Activation constant for IP_3 synthesis	0.6	Adjusted
d_{IP3}	IP_3 degradation rate	0.14 (s^{-1})	(Brown et al., 2008)

1. Rescaled means that the parameters from (De Pitta et al., 2008) are rescaled to yield appropriate amplitude and period of Ca^{2+} oscillations. Adjusted means that these parameters are adjusted by correlating the level of IP_3 with the stimulus strength between 0 to 1.

Table S2. Protein synthesis and degradation rates, related to Figure 1.

Parameter	Description	Value (Unit)	Reference
k_{Calp}	Synthesis rate of Calpain (Calp)	5.0×10^{-6} (μM/s)	(Hanna et al., 2008)
k_{Calc}	Synthesis rate of Calcineurin (Calc)	5.0×10^{-6} (μM/s)	(Bornhop et al., 2007)
k_{Cals}	Synthesis rate of Calpastatin (Cals)	1.25×10^{-6} (μM/s)	1/4 of Calp
k_{Bid}	Synthesis rate of Bid	5.3×10^{-6} (μM/s)	(Ballesta et al., 2013)
k_{pBad}	Synthesis rate of phosphorylated Bad (pBad)	1.0×10^{-5} (μM/s)	(Hekman et al., 2006)
k_{Bak}	Synthesis rate of Bak	1.0×10^{-4} (μM/s)	(Lindner et al., 2013)
k_{BclxL}	Synthesis rate of Bcl-X_L	2.5×10^{-5} (μM/s)	1/4 of Bak
k_{Cytcm}	Synthesis rate of Cyt c	1.3×10^{-1} (μM/s)	Deduced from (Rehm et al., 2006)
k_{Smacm}	Synthesis rate of Smac	1.6×10^{-3} (μM/s)	Deduced from (Rehm et al., 2006)
k_{Apaf}	Synthesis rate of Apaf-1	3.72×10^{-5} (μM/s)	(Rehm et al., 2006)
k_{pcasp9}	Synthesis rate of Procaspase 9	3.0×10^{-6} (μM/s)	(Rehm et al., 2006)
k_{pcasp3}	Synthesis rate of Procaspase 3	1.2×10^{-5} (μM/s)	(Rehm et al., 2006)
k_{XIAP}	Synthesis rate of XIAP	6.3×10^{-6} (μM/s)	(Rehm et al., 2006)
k_{PARP}	Synthesis rate of PARP	1.7×10^{-4} (μM/s)	(Rehm et al., 2006)
k_d	Degradation rate of all proteins and complexes	1.0×10^{-4} (1/s)	(Eden et al., 2011)

Table S3. Kinetic rate parameters, related to Figure 1.

Parameter	Description[1]	Value[2]	Corresponding reaction	Reference[3]
k_{1af}/ k_{1ar}	Association / Dissociation rate of Ca^{2+} and Calp	0.1 / 3.0	1~10	[4]
k_{1b1f}/ k_{1b1r}	Association / Dissociation rate of Ca^{2+} and Calc (the first two sites)	0.2 / 1.0	11, 12	[5]
k_{1b2f}/ k_{1b2r}	Association / Dissociation rate of Ca^{2+} and Calc (the last two sites)	200.0 / 1.0	13, 14	[5]
k_{2a1f}/ k_{2a1r}	Association / Dissociation rate of aCalp and Cals (the first site)	20.0 / 9.0×10^{-5}	15	[6]
k_{2a2f}/ k_{2a2r}	Association / Dissociation rate of aCalp and Cals (the second site)	3.0 / 0.01	16	[6]
k_{2a3f}/ k_{2a3r}	Association / Dissociation rate of aCalp and Cals (the third site)	5.0 / 0.003	17	[6]
k_{2a4f}/ k_{2a4r}	Association / Dissociation rate of aCalp and Cals (the fourth site)	6.0 / 3.0×10^{-4}	18	[6]
k_{2bf}/ k_{2br}	Association / Dissociation rate of aCalc and pBad	0.005 / 0.001	19	Adjusted
k_{2bcat}	Transition rate for Bad	1.0	19	[7]
k_{2cf}/ k_{2cr}	Association / Dissociation rate of aCalp and Bid	0.005 / 0.001	20	Adjusted
k_{2ccat}	Transition rate for tBid	1.0	20	[7]
K_{3cf}/ k_{3cr}	Association / Dissociation rate of tBid and Bak on the Mt	0.015 / 0.001	23	Adjusted
k_{3ccat}	Transition rate for aBak	1.0	23	[7]
k_{3d1f}/ k_{3d1r}	Association / Dissociation rate of aBak dimer on the Mt	0.6 / 0.001	24	[7]
k_{3d2f}/ k_{3d2r}	Association / Dissociation rate of two aBak dimers on the Mt	0.6 / 0.001	25	[7]
k_{3e1f}/ k_{3e1r}	Association / Dissociation rate of tBid and Bcl-X_L on the Mt	0.125 / 0.001	26	[8]
k_{3e2f}/ k_{3e2r}	Association / Dissociation rate of Bad and Bcl-X_L on the Mt	0.05 / 0.001	27	[8]
k_{3e3f}/ k_{3e3r}	Association / Dissociation rate of aBak and Bcl-X_L on the Mt	0.125 / 0.001	28	[8]
k_{3e4f}/ k_{3e4r}	Association / Dissociation rate of aBak dimer and Bcl-X_L on the Mt	0.125 / 0.001	29	[8]
k_{3e5f}/ k_{3e5r}	Association / Dissociation rate of aBak tetramer and Bcl-X_L on the Mt	0.125 / 0.001	30	[8]
v_{rel}	Maximum release rate of Cyt c and Smac from Mt	50000.0	31, 32	Adjusted
k_M	Release threshold of Cyt c and Smac	0.025	31, 32	Adjusted
p	Hill coefficient	5	31, 32	Adjusted
k_{4c1f} / k_{4c1r}	Association / Dissociation rate of Apaf-1 and Cyt c	0.04 / 0.001	33	[9]
k_{4c2f} / k_{4c2r}	Association / Dissociation rate of Apaf-1:Cyt c oligomers	10.0 / 0.001	34~37	[9]
k_{4df} / k_{4dr}	Association / Dissociation rate of Apoptosome and Procaspase 9	0.01 / 0.001	38	[9]
k_{4dcat}	Transition rate for Holoenzyme	1.0	38	[7]
k_{4ef} / k_{4er}	Association / Dissociation rate of Holoenzyme and Procaspase 3	1.0 / 0.001	39	[10]
k_{4ecat}	Transition rate for Caspase 3	0.17	39	[10]
k_{4f1f}/ k_{4f1r}	Association / Dissociation rate of Holoenzyme and XIAP	1.0 / 0.001	40	[9]
k_{4f2f}/ k_{4f2r}	Association / Dissociation rate of Caspase 3 and XIAP	1.0 / 0.001	41	[9]
k_{4f2cat}	XIAP-mediated destruction rate of Caspase 3	0.001	42	[11]
k_{4f3f}/ k_{4f3r}	Association / Dissociation rate of Smac and XIAP	3.0 / 0.001	43	[12]
k_{4gf}/ k_{4gr}	Association / Dissociation rate of Caspase 3 and PARP	0.6 / 0.01	44	[7]
k_{4gcat}	Transition rate for cPARP	1.0	44	[7]
k_{ctm}	Translocate rate for proteins from cytosol to Mt	0.01	21, 22	[13]
k_{mtc}	Translocate rate for proteins from Mt to cytosol	0.13	21, 22	[13]

1. Mt, mitochondria. Other abbreviations see Table S2.

2. All units are defined with respect to the cytosolic volume. Due to limited space, they are not listed here.

3. Adjusted means that these parameters are adjusted by matching the timescale of apoptosis to the experimental observations.

4. (Campbell and Davies, 2012); 5. (Li et al., 2011); 6. (Hanna et al., 2007); 7. (Albeck et al., 2008b); 8. (Ku et al., 2010); 9. (Würstle and Rehm, 2014); 10. (Pop et al., 2006); 11. (Albeck et al., 2008a); 12. (Huang et al., 2003); 13. (Aldridge et al., 2011).

Table S4. Biochemical reactions and corresponding reaction rates, related to Figure 1.

Number	Reaction	Reaction rate
1	$Calp+Ca^{2+}_{Mic} \underset{k_{1ar}}{\overset{k_{1af}}{\rightleftharpoons}} Calp1Ca$	$J_{1a1}=10k_{1af}[Calp][Ca^{2+}_{Mic}]-k_{1ar}[Calp1Ca]$
2~9	$CalpmCa + Ca^{2+}_{Mic} \underset{k_{1ar}}{\overset{k_{1af}}{\rightleftharpoons}} CalpnCa$ (m = 1 ~ 8, n = m + 1)	$J_{1an}=(11-n)k_{1af}[CalpmCa][Ca^{2+}_{Mic}]-k_{1ar}[CalpnCa]$
10	$Calp9Ca + Ca^{2+}_{Mic} \underset{k_{1ar}}{\overset{k_{1af}}{\rightleftharpoons}} aCalp$	$J_{1a10}=k_{1af}[Calp9Ca][Ca^{2+}_{Mic}]-k_{1ar}[aCalp]$
11	$Calc + Ca^{2+}_{Cyt} \underset{k_{1b1r}}{\overset{k_{1b1f}}{\rightleftharpoons}} Calc1Ca$	$J_{1b1}=2k_{1b1f}[Calc][Ca^{2+}_{Cyt}]-k_{1b1r}[Calc1Ca]$
12	$Calc1Ca + Ca^{2+}_{Cyt} \underset{k_{1b1r}}{\overset{k_{1b1f}}{\rightleftharpoons}} Calc2Ca$	$J_{1b2}=k_{1b1f}[Calc1Ca][Ca^{2+}_{Cyt}]-k_{1b1r}[Calc2Ca]$
13	$Calc2Ca + Ca^{2+}_{Cyt} \underset{k_{1b2r}}{\overset{k_{1b2f}}{\rightleftharpoons}} Calc3Ca$	$J_{1b3}=2k_{1b2f}[Calc2Ca][Ca^{2+}_{Cyt}]-k_{1b2r}[Calc3Ca]$
14	$Calc3Ca + Ca^{2+}_{Cyt} \underset{k_{1b2r}}{\overset{k_{1b2f}}{\rightleftharpoons}} aCalc$	$J_{1b4}=k_{1b2f}[Calc3Ca][Ca^{2+}_{Cyt}]-k_{1b2r}[aCalc]$
15	$Cals+aCalp \underset{k_{2a1r}}{\overset{k_{2a1f}}{\rightleftharpoons}} Cals:aCalp$	$J_{2a1}=k_{2a1f}[Cals][aCalp]-k_{2a1r}[Cals:aCalp]$
16	$Cals:aCalp+aCalp \underset{k_{2a2r}}{\overset{k_{2a2f}}{\rightleftharpoons}} Cals:aCalp_2$	$J_{2a2}=k_{2a2f}[Cals:aCalp][aCalp]-k_{2a2r}[Cals:aCalp_2]$
17	$Cals:aCalp_2+aCalp \underset{k_{2a3r}}{\overset{k_{2a3f}}{\rightleftharpoons}} Cals:aCalp_3$	$J_{2a3}=k_{2a3f}[Cals:aCalp_2][aCalp]-k_{2a3r}[Cals:aCalp_3]$
18	$Cals:aCalp_3+aCalp \underset{k_{2a4r}}{\overset{k_{2a4f}}{\rightleftharpoons}} Cals:aCalp_4$	$J_{2a4}=k_{2a4f}[Cals:aCalp_3][aCalp]-k_{2a4r}[Cals:aCalp_4]$
19	$aCalc+pBad \underset{k_{2br}}{\overset{k_{2bf}}{\rightleftharpoons}} aCalc:pBad \xrightarrow{k_{2bcat}} aCalc+Bad$	$J_{2b}=k_{2bf}[aCalc][pBad]-k_{2br}[aCalc:pBad]$ $J_{2bcat}=k_{2bcat}[aCalc:pBad]$
20	$aCalp+Bid \underset{k_{2cr}}{\overset{k_{2cf}}{\rightleftharpoons}} aCalp:Bid \xrightarrow{k_{2ccat}} aCalp+tBid$	$J_{2c}=k_{2cf}[aCalp][Bid]-k_{2cr}[aCalp:Bid]$ $J_{2ccat}=k_{2ccat}[aCalp:Bid]$
21	$tBid \underset{k_{mtc}}{\overset{k_{ctm}}{\rightleftharpoons}} tBid_m$	$J_{3atran}=k_{ctm}[tBid]-k_{mtc}[tBid_m]$
22	$Bad \underset{k_{mtc}}{\overset{k_{ctm}}{\rightleftharpoons}} Bad_m$	$J_{3btran}=k_{ctm}[Bad]-k_{mtc}[Bad_m]$
23	$tBid_m+Bak \underset{k_{3cr}}{\overset{k_{3cf}}{\rightleftharpoons}} tBid_m:Bak \xrightarrow{k_{3ccat}} tBid_m+aBak$	$J_{3c}=k_{3cf}/V[tBid_m][Bak]-k_{3cr}[tBid_m:Bak]$ $J_{3ccat}=k_{3ccat}[tBid_m:Bak]$
24	$2aBak \underset{k_{3d1r}}{\overset{k_{3d1f}}{\rightleftharpoons}} aBak_2$	$J_{3d1}=k_{3d1f}/V[aBak]^2-k_{3d1r}[aBak_2]$
25	$2aBak_2 \underset{k_{3d2r}}{\overset{k_{3d2f}}{\rightleftharpoons}} aBak_4$	$J_{3d2}=k_{3d2f}/V[aBak_2]^2-k_{3d2r}[aBak_4]$
26	$tBid_m+Bcl\text{-}X_L \underset{k_{3e1r}}{\overset{k_{3e1f}}{\rightleftharpoons}} tBid_m:Bcl\text{-}X_L$	$J_{3e1}=k_{3e1f}/V[tBid_m][Bcl\text{-}X_L]-k_{3e1r}[tBid_m:Bcl\text{-}X_L]$
27	$Bad_m+Bcl\text{-}X_L \underset{k_{3e2r}}{\overset{k_{3e2f}}{\rightleftharpoons}} Bad_m:Bcl\text{-}X_L$	$J_{3e2}=k_{3e2f}/V[Bad_m][Bcl\text{-}X_L]-k_{3e2r}[Bad_m:Bcl\text{-}X_L]$
28	$Bcl\text{-}X_L+aBak \underset{k_{3e3r}}{\overset{k_{3e3f}}{\rightleftharpoons}} Bcl\text{-}X_L:aBak$	$J_{3e3}=k_{3e3f}/V[Bcl\text{-}X_L][aBak]-k_{3e3r}[Bcl\text{-}X_L:aBak]$

29	$\text{Bcl-X}_L + \text{aBak}_2 \underset{k_{3e4r}}{\overset{k_{3e4f}}{\rightleftharpoons}} \text{Bcl-X}_L\text{:aBak}_2$	$J_{3e4} = k_{3e4f}/V[\text{Bcl-X}_L][\text{aBak}_2] - k_{3e4r}[\text{Bcl-X}_L\text{:aBak}_2]$
30	$\text{Bcl-X}_L + \text{aBak}_4 \underset{k_{3e5r}}{\overset{k_{3e5f}}{\rightleftharpoons}} \text{Bcl-X}_L\text{:aBak}_4$	$J_{3e5} = k_{3e5f}/V[\text{Bcl-X}_L][\text{aBak}_4] - k_{3e5r}[\text{Bcl-X}_L\text{:aBak}_4]$
31	$\text{Cyt c}_m \rightarrow \text{Cyt c}$	$J_{4atran} = v_{rel}\dfrac{[\text{MOMP}]^p}{k_M^p + [\text{MOMP}]^p}([\text{Cyt c}_m] - [\text{Cyt c}])$
32	$\text{Smac}_m \rightarrow \text{Smac}$	$J_{4btran} = v_{rel}\dfrac{[\text{MOMP}]^p}{k_M^p + [\text{MOMP}]^p}([\text{Smac}_m] - [\text{Smac}])$
33	$\text{Apaf} + \text{Cyt c} \underset{k_{4c1r}}{\overset{k_{4c1f}}{\rightleftharpoons}} \text{Apaf:Cyt c (AC)}$	$J_{4c1} = k_{4c1f}[\text{Apaf}][\text{Cyt c}] - k_{4c1r}[\text{AC}]$
34	$\text{AC} + \text{AC} \underset{k_{4c2r}}{\overset{k_{4c2f}}{\rightleftharpoons}} \text{AC}_2$	$J_{4c2} = k_{4c2f}[\text{AC}]^2 - k_{4c2r}[\text{AC}_2]$
35	$\text{AC} + \text{AC}_2 \underset{k_{4c2r}}{\overset{k_{4c2f}}{\rightleftharpoons}} \text{AC}_3$	$J_{4c3} = k_{4c2f}[\text{AC}][\text{AC}_2] - k_{4c2r}[\text{AC}_3]$
36	$\text{AC} + \text{AC}_3 \underset{k_{4c2r}}{\overset{k_{4c2f}}{\rightleftharpoons}} \text{AC}_4$	$J_{4c4} = k_{4c2f}[\text{AC}][\text{AC}_3] - k_{4c2r}[\text{AC}_4]$
37	$\text{AC}_3 + \text{AC}_4 \underset{k_{4c2r}}{\overset{k_{4c2f}}{\rightleftharpoons}} \text{Apop}$	$J_{4c5} = k_{4c2f}[\text{AC}_3][\text{AC}_4] - k_{4c2r}[\text{Apop}]$
38	$\text{Apop} + \text{pCasp9} \underset{k_{4dr}}{\overset{k_{4df}}{\rightleftharpoons}} \text{Apop:pCasp9} \xrightarrow{k_{4dcat}} \text{Holo}$	$J_{4d} = k_{4df}[\text{Apop}][\text{pCasp9}] - k_{4dr}[\text{Apop:pCasp9}]$ $J_{4dcat} = k_{4dcat}[\text{Apop:pCasp9}]$
39	$\text{Holo} + \text{pCasp3} \underset{k_{4er}}{\overset{k_{4ef}}{\rightleftharpoons}} \text{Holo:pCasp3} \xrightarrow{k_{4ecat}} \text{Holo} + \text{Casp3}$	$J_{4e} = k_{4ef}[\text{Holo}][\text{pCasp3}] - k_{4er}[\text{Holo:pCasp3}]$ $J_{4ecat} = k_{4ecat}[\text{Holo:pCasp3}]$
40	$\text{XIAP} + \text{Holo} \underset{k_{4f1r}}{\overset{k_{4f1f}}{\rightleftharpoons}} \text{XIAP:Holo}$	$J_{4f1} = k_{4f1f}[\text{XIAP}][\text{Holo}] - k_{4f1r}[\text{XIAP:Holo}]$
41	$\text{XIAP} + \text{Casp3} \underset{k_{4f2r}}{\overset{k_{4f2f}}{\rightleftharpoons}} \text{XIAP:Casp3}$	$J_{4f2} = k_{4f2f}[\text{XIAP}][\text{Casp3}] - k_{4f2r}[\text{XIAP:Casp3}]$
42	$\text{XIAP:Casp3} \xrightarrow{k_{4f2cat}} \phi$	$J_{4f2cat} = k_{4f2cat}[\text{XIAP:Casp3}]$
43	$2\text{Smac} + \text{XIAP} \underset{k_{4f3r}}{\overset{k_{4f3f}}{\rightleftharpoons}} \text{Smac}_2\text{:XIAP}$	$J_{4f3} = k_{4f3f}[\text{Smac}]^2[\text{XIAP}] - k_{4f3r}[\text{Smac}_2\text{:XIAP}]$
44	$\text{Casp3} + \text{PARP} \underset{k_{4gr}}{\overset{k_{4gf}}{\rightleftharpoons}} \text{Casp3:PARP} \xrightarrow{k_{4gcat}} \text{Casp3} + \text{cPARP}$	$J_{4g} = k_{4gf}[\text{Casp3}][\text{PARP}] - k_{4gr}[\text{Casp3:PARP}]$ $J_{4gcat} = k_{4gcat}[\text{Casp3:PARP}]$

Table S5. Ordinary differential equations, related to Figure 1.

Number	ODE
1	$\dot{[Calp]}=k_{Calp}-J_{1a1}-k_d[Calp]$
2	$\dot{[Calp1Ca]}=J_{1a1}-J_{1a2}-k_d[Calp1Ca]$
3	$\dot{[Calp2Ca]}=J_{1a2}-J_{1a3}-k_d[Calp2Ca]$
4	$\dot{[Calp3Ca]}=J_{1a3}-J_{1a4}-k_d[Calp3Ca]$
5	$\dot{[Calp4Ca]}=J_{1a4}-J_{1a5}-k_d[Calp4Ca]$
6	$\dot{[Calp5Ca]}=J_{1a5}-J_{1a6}-k_d[Calp5Ca]$
7	$\dot{[Calp6Ca]}=J_{1a6}-J_{1a7}-k_d[Calp6Ca]$
8	$\dot{[Calp7Ca]}=J_{1a7}-J_{1a8}-k_d[Calp7Ca]$
9	$\dot{[Calp8Ca]}=J_{1a8}-J_{1a9}-k_d[Calp8Ca]$
10	$\dot{[Calp9Ca]}=J_{1a9}-J_{1a10}-k_d[Calp9Ca]$
11	$\dot{[aCalp]}=J_{1a10}-J_{2a1}-J_{2a2}-J_{2a3}-J_{2a4}-J_{2c}+J_{2ccat}-k_d[aCalp]$
12	$\dot{[Calc]}=k_{Calc}-J_{1b1}-k_d[Calc]$
13	$\dot{[Calc1Ca]}=J_{1b1}-J_{1b2}-k_d[Calc1Ca]$
14	$\dot{[Calc2Ca]}=J_{1b2}-J_{1b3}-k_d[Calc2Ca]$
15	$\dot{[Calc3Ca]}=J_{1b3}-J_{1b4}-k_d[Calc3Ca]$
16	$\dot{[aCalc]}=J_{1b4}-J_{2b}+J_{2bcat}-k_d[aCalc]$
17	$\dot{[Cals]}=k_{Cals}-J_{2a1}-k_d[Cals]$
18	$\dot{[Cals:aCalp]}=J_{2a1}-J_{2a2}-k_d[Cals:aCalp]$
19	$\dot{[Cals:aCalp_2]}=J_{2a2}-J_{2a3}-K_d[Cals:aCalp_2]$
20	$\dot{[Cals:aCalp_3]}=J_{2a3}-J_{2a4}-k_d[Cals:aCalp_3]$
21	$\dot{[Cals:aCalp_4]}=J_{2a4}-k_d[Cals:aCalp_4]$
22	$\dot{[pBad]}=k_{pBad}-J_{2b}-k_d[pBad]$
23	$\dot{[aCalc:pBad]}=J_{2b}-J_{2bcat}-k_d[aCalc:pBad]$

24 $$\dot{[Bad]}=J_{2bcat}-J_{3btran}-k_d[Bad]$$

25 $$\dot{[Bad_m]}=J_{3btran}-J_{3e2}-k_d[Bad_m]$$

26 $$\dot{[Bid]}=k_{Bid}-J_{2c}-k_d[Bid]$$

27 $$\dot{[aCalp:Bid]}=J_{2c}-J_{2ccat}-k_d[aCalp:Bid]$$

28 $$\dot{[tBid]}=J_{2ccat}-J_{3atran}-k_d[tBid]$$

29 $$\dot{[tBid_m]}=J_{3atran}-J_{3c}+J_{3ccat}-k_d[tBid_m]$$

30 $$\dot{[Bak]}=k_{Bak}-J_{3c}-k_d[Bak]$$

31 $$\dot{[tBid_m:Bak]}=J_{3c}-J_{3ccat}-k_d[tBid_m:Bak]$$

32 $$\dot{[aBak]}=J_{3ccat}-2J_{3d1}-J_{3e3}-k_d[aBak]$$

33 $$\dot{[aBak_2]}=J_{3d1}-2J_{3d2}-J_{3e4}-k_d[aBak_2]$$

34 $$\dot{[aBak_4]}=J_{3d2}-J_{3e5}-k_d[aBak_4]$$

35 $$\dot{[Bcl\text{-}X_L]}=k_{Bcl\text{-}X_L}-J_{3e1}-J_{3e2}-J_{3e3}-J_{3e4}-J_{3e5}-k_d[Bcl\text{-}X_L]$$

36 $$\dot{[tBid_m:Bcl\text{-}X_L]}=J_{3e1}-k_d[tBid_m:Bcl\text{-}X_L]$$

37 $$\dot{[Bad_m:Bcl\text{-}X_L]}=J_{3e2}-k_d[Bad_m:Bcl\text{-}X_L]$$

38 $$\dot{[Bcl\text{-}X_L:aBak]}=J_{3e3}-k_d[Bcl\text{-}X_L:aBak]$$

39 $$\dot{[Bcl\text{-}X_L:aBak_2]}=J_{3e4}-k_d[Bcl\text{-}X_L:aBak_2]$$

40 $$\dot{[Bcl\text{-}X_L:aBak_4]}=J_{3e5}-k_d[Bcl\text{-}X_L:aBak_4]$$

41 $$\dot{[Cyt\ c_m]}=k_{Cyt\ c_m}-J_{4atran}-k_d[Cyt\ c_m]$$

42 $$\dot{[Smac_m]}=k_{Smac_m}-J_{4btran}-k_d[Smac_m]$$

43 $$\dot{[Cyt\ c]}=VDV*J_{4atran}-J_{4c1}-k_d[Cyt\ c]$$

44 $$\dot{[Smac]}=VDV*J_{4btran}-2J_{4f3}-k_d[Smac]$$

45 $$\dot{[Apaf]}=k_{Apaf}-J_{4c1}-k_d[Apaf]$$

46 $$\dot{[AC]}=J_{4c1}-2J_{4c2}-J_{4c3}-J_{4c4}-k_d[AC]$$

47 $$\dot{[AC_2]}=J_{4c2}-J_{4c3}-k_d[AC_2]$$

48 $$\dot{[AC_3]}=J_{4c3}-J_{4c4}-J_{4c5}-k_d[AC_3]$$

49 $$\dot{[AC_4]}=J_{4c4}-J_{4c5}-k_d[AC_4]$$

50 $$\dot{[Apop]}=J_{4c5}-J_{4d}-k_d[Apop]$$

51 $$\dot{[pCasp9]}=k_{pCasp9}-J_{4d}-k_d[pCasp9]$$

52 $$\dot{[Apop:pCasp9]}=J_{4d}-J_{4dcat}-k_d[Apop:pCasp9]$$

53 $$\dot{[Holo]}=J_{4dcat}-J_{4e}+J_{4ecat}-J_{4f1}-k_d[Holo]$$

54 $$\dot{[pCasp3]}=k_{pCasp3}-J_{4e}-k_d[pCasp3]$$

55 $$\dot{[Holo:pCasp3]}=J_{4e}-J_{4ecat}-k_d[Holo:pCasp3]$$

56 $$\dot{[Casp3]}=J_{4ecat}-J_{4f2}-J_{4g}+J_{4gcat}-k_d[Casp3]$$

57 $$\dot{[XIAP]}=k_{XIAP}+J_{4f2cat}-J_{4f1}-J_{4f2}-J_{4f3}+J_{4f2cat}-k_d[XIAP]$$

58 $$\dot{[XIAP:Holo]}=J_{4f1}-k_d[XIAP:Holo]$$

59 $$\dot{[XIAP:Casp3]}=J_{4f2}-J_{4f2cat}-k_d[XIAP:Casp3]$$

60 $$\dot{[Smac:XIAP]}=J_{4f3}-k_d[Smac:XIAP]$$

61 $$\dot{[PARP]}=k_{PARP}-J_{4g}-k_d[PARP]$$

62 $$\dot{[Casp3:PARP]}=J_{4g}-J_{4gcat}-k_d[Casp3:PARP]$$

63 $$\dot{[cPARP]}=J_{4gcat}-k_d[cPARP]$$

64 $$\dot{[IP3]}=p_{IP3}\frac{Stimulus^2}{k_{IP3}^2+Stimulus^2}-d_{IP3}[IP_3]$$

65 $$\dot{h}=\alpha_h(1-h)-\beta_h h$$

66 $$\begin{aligned}\dot{[Ca\_cyt]}=&(J_{IP3R}+J_{Leak}-J_{SERCA})-\sum_1^{10}J_{1ai}-\sum_1^{4}J_{1bj}\\&+k_d\sum_1^{9}m[CalpmCa]+10k_d[aCalp]\\&+k_d\sum_1^{3}n[CalcnCa]+4k_d[aCalc]\\&+10k_d(\sum_1^{4}q[Cals:aCalp_q]+[aCalp:Bid])\\&+4k_d[aCalc:pBad]\end{aligned}$$

Supplemental References

Albeck, J.G., Burke, J.M., Aldridge, B.B., Zhang, M., Lauffenburger, D.A., and Sorger, P.K. (2008a). Quantitative analysis of pathways controlling extrinsic apoptosis in single cells. Mol. Cell *30*, 11-25.

Albeck, J.G., Burke, J.M., Spencer, S.L., Lauffenburger, D.A., and Sorger, P.K. (2008b). Modeling a snap-action, variable-delay switch controlling extrinsic cell death. PLoS Biol. *6*, e299.

Aldridge, B., Gaudet, S., Lauffenburger, D., and Sorger, P. (2011). Lyapunov exponents and phase diagrams reveal multi-factorial control over TRAIL-induced apoptosis. Mol. Syst. Biol. *7*, 553.

Ballesta, A., Lopez, J., Popgeorgiev, N., Gonzalo, P., Doumic, M., and Gillet, G. (2013). Data-driven modeling of SRC control on the mitochondrial pathway of apoptosis: implication for anticancer therapy optimization. PLoS Comput. Biol. *9*, e1003011.

Bornhop, D.J., Latham, J.C., Kussrow, A., Markov, D.A., Jones, R.D., and Sørensen, H.S. (2007). Free-solution, label-free molecular interactions studied by back-scattering interferometry. Science *317*, 1732-1736.

Brown, S.-A., Morgan, F., Watras, J., and Loew, L.M. (2008). Analysis of phosphatidylinositol-4,5-bisphosphate signaling in cerebellar purkinje spines. Biophys. J. *95*, 1795-1812.

Campbell, R.L., and Davies, P.L. (2012). Structure–function relationships in calpains. Biochem. J. *447*, 335-351.

Chang, Y., Bruni, R., Kloss, B., Assur, Z., Kloppmann, E., Rost, B., Hendrickson, W.A., and Liu, Q. (2014). Structural basis for a pH-sensitive calcium leak across membranes. Science *344*, 1131-1135.

Chen, M., He, H., Zhan, S., Krajewski, S., Reed, J.C., and Gottlieb, R.A. (2001). Bid is cleaved by calpain to an active fragment in vitro and during myocardial ischemia/reperfusion. J. Biol. Chem. *276*, 30724-30728.

De Pitta, M., Volman, V., Levine, H., Pioggia, G., De Rossi, D., and Benjacob, E. (2008). Coexistence of amplitude and frequency modulations in intracellular calcium dynamics. Phys. Rev. E *77*, 030903.

Eden, E., Geva-Zatorsky, N., Issaeva, I., Cohen, A., Dekel, E., Danon, T., Cohen, L., Mayo, A., and Alon, U. (2011). Proteome half-life dynamics in living human cells. Science *331*, 764-768.

Flusberg, D.A., and Sorger, P.K. (2015). Surviving apoptosis: life–death signaling in single cells. Trends Cell Biol. *25*, 446-458.

Garcia, M.I., Chen, J.J., and Boehning, D. (2017). Genetically encoded calcium indicators for studying long-term calcium dynamics during apoptosis. Cell Calcium *61*, 44-49.

Giacomello, M., Drago, I., Bortolozzi, M., Scorzeto, M., Gianelle, A., Pizzo, P., and Pozzan, T. (2010). Ca^{2+} hot spots on the mitochondrial surface are generated by Ca^{2+} mobilization from stores, but not by activation of store-operated Ca^{2+} channels. Mol. Cell *38*, 280-290.

Ginzberg, M.B., Kafri, R., and Kirschner, M. (2015). On being the right (cell) size. Science *348*, 1245075.

Giorgi, C., Danese, A., Missiroli, S., Patergnani, S., and Pinton, P. (2018). Calcium dynamics as a machine for decoding signals. Trends Cell Biol. *28*, 258-273.

Hanna, R.A., Campbell, R.L., and Davies, P.L. (2008). Calcium-bound structure of calpain and its mechanism of inhibition by calpastatin. Nature *456*, 409-412.

Hanna, R.A., Garcia-Diaz, B.E., and Davies, P.L. (2007). Calpastatin simultaneously binds four calpains with different kinetic constants. FEBS Lett. *581*, 2894-2898.

Harr, M.W., and Distelhorst, C.W. (2010). Apoptosis and autophagy: decoding calcium signals that mediate life or death. CSH Perspect. Biol. *2*, a005579.

Hekman, M., Albert, S., Galmiche, A., Rennefahrt, U.E.E., Fueller, J., Fischer, A., Puehringer, D., Wiese, S., and Rapp, U.R. (2006). Reversible membrane interaction of Bad requires two C-terminal lipid binding domains in conjunction with 14-3-3 protein binding. J. Biol. Chem. *281*, 17321-17336.

Huang, Y., Rich, R., Myszka, D., and Wu, H. (2003). Requirement of both the second and third BIR domains for the relief of X-linked inhibitor of apoptosis protein (XIAP)-mediated caspase inhibition by Smac. J. Biol. Chem. *278*, 49517-49522.

Ku, B., Liang, C., Jung, J.U., and Oh, B.-H. (2010). Evidence that inhibition of BAX activation by BCL-2 involves its tight and

preferential interaction with the BH3 domain of BAX. Cell Res. *21*, 627-641.

Li, H., Rao, A., and Hogan, P.G. (2011). Interaction of calcineurin with substrates and targeting proteins. Trends Cell Biol. *21*, 91-103.

Lindner, A.U., Prehn, J.H.M., and Huber, H.J. (2013). The indirect activation model of mitochondrial outer membrane permeabilisation (MOMP) initiation requires a trade-off between robustness in the absence of and sensitivity in the presence of stress. Mol. Biosyst. *9*, 2359-2369.

Liu, X., Wang, X., Yang, X., Liu, S., Jiang, L., Qu, Y., Hu, L., Ouyang, Q., and Tang, C. (2015). Reliable cell cycle commitment in budding yeast is ensured by signal integration. Elife *4*, e03977.

Moldoveanu, T., Gehring, K., and Green, D.R. (2008). Concerted multi-pronged attack by calpastatin to occlude the catalytic cleft of heterodimeric calpains. Nature *456*, 404-408.

Monteith, G.R., Prevarskaya, N., and Roberts-Thomson, S.J. (2017). The calcium-cancer signalling nexus. Nat. Rev. Cancer *17*, 367-380.

Morigi, M., Perico, L., Rota, C., Longaretti, L., Conti, S., Rottoli, D., Novelli, R., Remuzzi, G., and Benigni, A. (2015). Sirtuin 3–dependent mitochondrial dynamic improvements protect against acute kidney injury. J. Clin. Invest. *125*, 715-726.

Pop, C., Timmer, J., Sperandio, S., and Salvesen, G. (2006). The apoptosome activates caspase-9 by dimerization. Mol. Cell *22*, 269-275.

Qi, H., Jiang, Y., Yin, Z., Jiang, K., Li, L., and Shuai, J. (2018). Optimal pathways for the assembly of the Apaf-1·cytochrome c complex into apoptosome. Phys. Chem. Chem. Phys. *20*, 1964-1973.

Rehm, M., Huber, H.J., Dussmann, H., and Prehn, J.H. (2006). Systems analysis of effector caspase activation and its control by X-linked inhibitor of apoptosis protein. EMBO J. *25*, 4338-4349.

Scorrano, L., Oakes, S.A., Opferman, J.T., Cheng, E.H., Sorcinelli, M.D., Pozzan, T., and Korsmeyer, S.J. (2003). Bax and Bak regulation of endoplasmic reticulum Ca^{2+}: a control point for apoptosis. Science *300*, 135-139.

Wang, H.-G., Pathan, N., Ethell, I.M., Krajewski, S., Yamaguchi, Y., Shibasaki, F., McKeon, F., Bobo, T., Franke, T.F., and Reed, J.C. (1999). Ca^{2+}-induced apoptosis through calcineurin dephosphorylation of BAD. Science *284*, 339-343.

Würstle, M.L., and Rehm, M. (2014). A systems biology analysis of apoptosome formation and apoptosis execution supports allosteric procaspase-9 activation. J. Biol. Chem. *289*, 26277-26289.

Zhao, L., Sun, T., Pei, J., and Ouyang, Q. (2015). Mutation-induced protein interaction kinetics changes affect apoptotic network dynamic properties and facilitate oncogenesis. Proc. Natl. Acad. Sci. USA *112*, E4046-E4054.